1976

A study of some aspects of conditioning coal flyash for electrostatic precipitation

Michael W. Neff
Lehigh University

A Study of Some Aspects of Conditioning Coal Flyash for Electrostatic Precipitation

by

Michael W. Neff

A Research Report
Presented to the Graduate Faculty
of Lehigh University
in Candidacy for the Degree of
Master of Science
in
Chemical Engineering

Lehigh University
June 1976

Certificate of Approval

This research report is accepted and approved in partial fullfillment of the requirements for the degree of Master of Science in Chemical Engineering.

(date)

Dr. Robert W. Coughlin
Professor in Charge

Dr. Leonard A. Wenzel
Chairman of the Department
of Chemical Engineering

Acknowledgements

I am indebted to many individuals for their valuable help during the course of this undertaking. First and foremost, I would like to thank Dr. R. W. Coughlin for his patience and guidance. Many thanks go to Dr. J. I. Goldstein, D. Korastinsky, D. Bush and B. Smith for their help with the microscopy work. Thanks also go to J. Hojsak for his assistance in the construction of the sulfur oxide detector and other experimental apparatus.

I gratefully acknowledge the financial support of the Middle Atlantic Power Research Committee and the National Science Foundation.

To Nan, may her world always be as beautiful as she has made mine.

and

To my parents for their love, patience and understanding.

Table of Contents

Nomenclature

K	total electrical conductivity of glass beads, $\Omega^{-1}cm^{-1}$
K_v	electrical conductivity of dry glass beads, $\Omega^{-1}cm^{-1}$
K_s	effective electrical conductivity of capillary condensed liquid, $\Omega^{-1}cm^{-1}$
p_o	saturated vapor pressure of capillary condensed or adsorbed compound, psi
p_k	vapor pressure of capillary condensed or adsorbed compound, psi
k	length of contact between two particles
d_p	particle diameter, m
	electrical resistivity, Ω-cm
ρ_s	effective resistivity of capillary condensed liquid Ω-cm
α	contact angle
C_v	absolute volumetric concentration of H_2O in air or flue gas, $\%H_2O$

Abstract

The effect of SO_3 in improving electrostatic precipitator efficiency of low sulfur coal flyash has been known for some time. The scanning electron microscope and electron microprobe have been used to try to determine the role SO_3 plays in the precipitation process. Sulfur was found on the surface of flyash particles, but no sulfur could be detected in the inner portions of the particles.

Some materials that could be possible substitutes for SO_3 in the flyash conditioning process for electrostatic precipitation were investigated. NaCl, $CaCl_2$ and $PbSO_4$ waste were found to have little or no effect on flyash resistivity. Sulfamic acid, wet scrubber underflow and weak ammonia liquor were found to affect the flyash resistivity significantly.

A sulfur oxide detector was built to monitor sulfur oxide concentrations. The instrument was based on flame photometry with H_2 as the fuel. Light emitted from S_2 in the 3100-3300 angstrom range was isolated and detected with a photomultiplier tube. The instrument had a detectability limit of 900ppm (by volume) and a resolution of about ±100 ppm. A possible improvement in detection capabilities has been suggested.

An attempt to verify the model recently proposed by

Ditl and Coughlin that explains the dependency of flyash resistivity with temperature and flue gas composition has been made. The resistivity of a bed of spherical glass beads was measured as a function of temperature and humidity. Theoretical curves of log resistivity versus temperature were generated using the proposed model. Comparison of the theoretical and experimental curves indicate that the model is at least partially successful in describing the process of electrical conduction in a layer of spherical particles.

Flyash Conditioning Experiments

While SO_3 is known to be a good conditioning agent for the electrostatic precipitation of flyash, it is toxic, corrosive, expensive and itself a pollutant. Because of these difficulties it was decided to investigate the conditioning effects of other materials. The materials tested were NaCl, $CaCl_2$, sulfamic acid, a lead sulfate waste liquor from batteries, a wet scrubber underflow (calcium sulfate) and a weak ammonia waste liquor from the coke operations of Bethlehem Steel Corporation.

Experimental

All materials were tested in the apparatus diagrammed in Figure 1. Flue gas was produced by burning natural gas in a gas burner(1) and convected through the 2 inch diameter pipe by the gas blower(2). The conditioning agents were metered into the gas stream at a point just beyond the gas burner(4). Flyash obtained from the Front Street Station (Erie, PA) of the Pennsylvania Electric Company was packed into a layer about 4 mm. thick on the lower electrode shown in Figure 1. An upper electrode disk was then lowered onto the flyash surface and 4000 volts was applied to the upper electrode by a Spellman High-Voltage Power Supply Model 20 PN 30. Current flow through the flyash was measured with a Keithley Electrometer 610C. The flue gas

temperature near the gas burner and at the flyash bed was measured with thermocouples and recorded on a Honeywell recorder.

Information as to the various solutions fed into the flue gas is summarized in Table 1. The effect of adding these solutions to the flue gas on the resistivity of the flyash is shown in Figures 2, 3 and 4. Each curve of resistivity versus time is labelled as to the solution employed.

Results and Discussion

The resistivity versus time curves shown in Figure 2 for NaCl, $CaCl_2$ and in Figure 3 for $PbSO_4$ waste show that these materials have little effect on the resistivity of the flyash. In fact the only noticeable effect is a slight increase in resistivity upon the addition of each of these three materials. NaCl, $CaCl_2$ and $PbSO_4$ waste obviously are poor conditioning agents.

On the other hand, the results for the other three materials, weak ammonia liquor, wet scrubber underflow, and sulfamic acid are more promising. The resistivity versus time curve for weak ammomia liquor , shown in Figure 2 , appears to be very similar to that for SO_3 , shown in Figure 5 , in that there is a gradual drop in resistivity upon the addition of the conditioning agent

and then a gradual rise in resistivity to the original level as soon as the conditioning agent is stopped. However , for the conditions under which the ammonia liquor was added , the overall decrease in resistivity is not nearly as extensive nor as rapid as that normally observed with SO_3 .

By contrast both the wet scrubber underflow and sulfamic acid resistivity versus time curves , shown in Figures 3 and 4 respectively , exhibit characteristics markedly different from the SO_3 curve. Upon addition of the wet scrubber underflow , the flyash resistivity immediately dropped to a low level and then remained near that level. Subsequent addition of SO_3 did not produce any major change in the flyash resistivity. The wet scrubber underflow acts differently from SO_3 in two ways. First the addition of the scrubber underflow causes an immediate , large drop in resistivity as compared to the gradual change in resistivity caused by SO_3. The resistivity versus time curve for sulfamic acid shows the same gradual decrease in resistivity that is seen in the SO_3 system. There is no rise in resistivity , however , when the sulfamic acid flow is cut off. In this way sulfamic acid is similar to the wet scrubber underflow. Again this behavior may suggest the possibility of a conditioning mechanism different from that exhibited by SO_3.

Microscopy of Flyash

While it is known that a small amount of SO_3 in the flue gas reduces the electrical resistivity of flyash, the mechanism by which this phenomenom occurs has not been clearly established. One theory is that SO_3 is adsorbed on to the flyash surface and forms a conductive film. Another possibility is that the SO_3 actually diffuses into the flyash particles and contributes directly to the conduction process via ion migration. If this latter situation occurs, there should be a sulfur concentration gradient into particles that have been conditioned with SO_3 that could possibly be detected and measured with an electron microprobe.

As a preliminary effort, a general characterization of the flyash particles by scanning electron microscopy (SEM) and light microscopy was attempted. The study of flyash properties by microscopy is not new; a number of similar attempts have been made in the past to characterize these properties[1,2]. Due to the complex heterogeneous nature of flyash, however, these previous attempts produced essentially only qualitative descriptions. Although most of the preliminary work reported here is also of a qualitative nature, quantitative results have also been obtained using a solid-state x-ray detector in conjunction with the scanning electron microscope to identify

elements present on the surface only in concentrations greater than 1% by mass.

Sample Preparation SEM

Mounting flyash samples for SEM work is a relatively simple task. In the procedure used, formvar (.05 wt. %) in diethylenechloride was spread evenly across the surface of an aluminum stub; then flyash was lightly sprinkled on the stub, with care taken to obtain a relatively large separation of particles. After drying the sample was coated with carbon. This carbon coating provides a conduction path for the electrons from the microscope electron beam. Without this conduction path, charge buildup would occur, producing a distorted image[3].

Sample Preparation: Electron Microprobe Analysis

Flyash sample preparation for electron microprobe analysis (EMPA) is much more complicated than preparation for analysis by SEM. The critical requirement in EMPA is that the sample have a flat surface. If the sample surface is irregular, some x-rays will be absorbed by the irregularities of the surface, causing an error in the analysis[3]. The sample surface is made regular by polishing. Since the flyash particles are small, they must be mounted in a block of material in order to be able to perform the polishing

step.

Two types of mounting were used at various times throughout the investigation. The first type is a "cold mount" method involving the use of an epoxy resin. In this method a glass plate is covered with a silicon release agent. Then a bakelite ringform that has an outer diameter of one inch and is about three quarters of an inch high is placed upon the glass plate. The flyash is lightly sprinkled, with as much particle separation as possible, on the glass within the ring. Next, Buehler epoxide resin #20-8132 is mixed with Buehler epoxide hardener #20-8130 and this mixture is poured into the ringform to a height of about one half of an inch. A weight is placed on top of the ringform so that epoxy can not seep out from the bottom of the ring. The sample is then set aside to allow curing of the epoxy for about 8 hours.

In the "hot mount" procedure the mold consists of a hollow steel cylinder several inches long and 1 1/4 inches in diameter and two solid steel cylinders to serve as endpieces for the hollow cylinder. The flyash is lightly sprinkled on the inside face of the solid cylinder that will serve as the bottom of the mold. The hollow cylinder is placed around the bottom piece. The mounting material, Buehler Transoptic, is poured in until it fills about half of the mold. Then the top cylinder is put in place. A

heating jacket is placed around the mold and the mold is put in a press. The sample is then heated to a temperature of 300°C and 4200 psi of pressure is applied. After 25 minutes under these conditions the heat input is removed. When the sample cools to about 150°C, the applied pressure is removed and when the mold is cool enough to touch, the sample is removed. The "hot mount" method is easier, faster and seems to produce better samples than that of the "cold mount" method.

In the subsequent operation, that of polishing the sample, the initial step is to grind the sample with wetted silicon carbide grinding paper, 320-A grit, and then wash the sample with water. Then the sample is rotated 90 and ground again with a 400-A grit silicon carbide paper until all the marks left from the previous paper are removed. After washing the sample is again rotated 90 and ground with a 600 grit silicon carbide grinding paper until all the marks caused by the 400 grit paper are removed.

After the above steps and a rinse with water the sample is polished with diamond paste. A nylon polishing cloth is placed over a piece of plate glass and a small amount of 6 micron Buehler Metadi Diamond Compound is placed on the cloth and mixed with several drops of Buehler Metadi Fluid Extender to form a thick paste. The sample is then rubbed in a circular motion in the paste for

several minutes, after which the sample is washed thoroughly with water. This procedure isrepeated with a 1 micron metadi compound. After washing with water the degree of polish is checked with an optical microscope. If the polishing job is insufficient, the above procedure should be repeated (it is normally sufficient to repeat just the diamond paste polishing steps.)

Since there are many particles mounted into a single sample, the fianl preparation step involves photographing the sample so that a "map" of the particles may be developed. This map is then used along with the photographs to identify and locate particles of interest for the electron microprobe analysis. A Zeiss reflected light microscope and Polaroid camera were used to take the pictures. Figure 6 shows a typical sample of polished flyash.

Experimental

The scanning electron micrscopy was done on an ETEC Autoscan Model U1 at a voltage of 20 KV. A solid-state x-ray detector was used in conjunction with the scanning electron microscope. The solid-state x-ray detector could provide only qualitative information as to which elements were present on the particle surface in quantities greater than 1% by mass.

The electron microprobe analysis was done on an

Applied Research Labs EMX-SM. The microprobe was operated at a voltage of 15 KV and a current of .15 mA and the electron beam spot size was about 1 micron in diameter. The electron microprobe was equipped with crystal diffraction spectrometers (CDS) which are much more sensitive than the solid-state x-ray detectors. The CDS operate by the principles of Bragg's Law and the crystals can be tuned to the wavelength emitted by a specific element. X-ray pulses from a given sample can be monitired, counted and compared to the pulse count obtained from a standard of known concentration in the element of interest. The electron beam was traversed across a particle so that the analysis could be made every 4 microns. An additional sweep of the sample along a line perpendicular to the first sweep was also made. For this system and procedure it was calculated that the x-ray pulse count for a particular point must exceed the background count by 60 to insure that sulfur was present with 95% confidence.

Results and Discussion

Optical Microscopy

Polished flyash was examined with a reflected light microscope in an attempt to identify the minerals present. As a result the particles could be classified in four groups.

The first group consisted of particles that reflected light, i.e., those particles that appeared white. The second group consisted of gray spherical particles with some dark spots on them. A third group of particles consisted of small black chips. Irregularly shaped particles of various colors made up the fourth group. Particles of all four groups are shown in Figure 6. Unfortunately, only the first group of particles could be identified with reflected light microscopy. Under polarized light the white particles turned orange and ruby red, indicating that those particles consisted of the iron oxides hematite and magnatite. However the group I particles make up a small fraction of the total amount of flyash examined. Thus the bulk of the flyash remained unidentifiable by reflected light microscopy. Nevertheless, the particle classification system combined with the sample "maps" made the electron microprobe analysis more orderly.

SEM

The first sample examined was sieved dry to obtain a size fraction of 53 microns to 105 microns. Photographs taken on the scanning electron micrscope of particles that are representative of this sample are shown in Figures 7, 8 and 9. Some Front Street flyash was also wet sieved (with H_2O) in an attempt to obtain a better separation of particle sizes. Figures 10 and 11 show wet sieved flyash from the

53 to 105 micron fraction while Figures 12 and 13 show flyash from the 44 to 53 micron fraction. All these photographs show that there are two types of particles present, small glassy spheres and larger porous particles. The large porous particles seem to consist of the smaller glassy spheres surrounded by a glassy shell. The energy dispersive x-ray analysis of these particles is shown in Table 2. The analysis shows that all particles, regardless of size, contain Al, Si, K, Ti and Fe in quantities greater than 1% by mass.

Another flyash sample was first exposed to SO_3 and then examined with the scanning electron microscope. Figures 14, 15 and 16 contain photomicrographs of this sample. The SO_3 exposure apparently had no structural effect on the flyash, as there were no visual differences between the conditioned and unconditioned samples. However, the x-ray analysis showed that sulfur was present on the surface of the conditioned sample. This result indicates that SO_3 had either reacted with or been adsorbed on to the flyash. Electron microprobe analysis was then employed in an attempt to learn how the deposited sulfur was spatially distributed within the particles.

Electron Microprobe Analysis

Both unconditioned and SO_3 conditioned flyash were

examined with the electron microprobe. However, the first samples examined showed no traces of sulfur in either the conditioned or unconditioned flyash. This result was surprising since all flyash should contain a certain amount of residual sulfur. Subsequently it was decided that the sulfur was being extracted by the water used in the polishing process. To prevent such extraction n-heptane was substituted for water in the polishing procedure and new samples were prepared.

Figures 17-21 show photographs of unconditioned Front Street Station flyash that has been prepared for electron microprobe analysis. Seven of the particles examined are marked on the photographs. Table 3 shows the x-ray pulse counts for the elements Fe, S and Na for these particular particles and background.

Photographs of SO_3 conditioned Front Street flyash that has been prepared for microprobe analysis are shown in Figures 22-25. Ten of the particles examined are marked on the photographs in these Figures. Table 4 contains the x-ray pulse count data for these particles and background for the elements Fe, S and Na.

The data in Table 4 shows that there are very few points in either the treated or untreated samples that show indications of the presence of sulfur. The few points

that were detected are most likely points containing some residual sulfur. While the SEM study showed that sulfur was on the surface of the conditioned flyash particles, the electron microprobe analysis indicates that there is little or no tendency for the sulfur to diffuse in to the bulk of the particles.

Sulfur Oxide Analysis: Flame Photometry

One of the major problems encountered in a study involving a sulfur oxide-air mixture is the analytical determination of the sulfur oxide concentration, especially at low concentration levels. One common analytical technique recommended by the EPA involves a titration analysis. However, there are several difficulties encountered with this method. Samples have to be collected by drawing off a gas stream and bubbling it through several impingers with solvents to absorb the sulfur oxides. The efficiency of this collection system is questionable. The major problem howevere lies with the titration analysis itself. The titration end point is a yellow to orange color change that is very hard to see. When low concentrations are involved, the uncertainty of the end point can contribute to a large error in the final result. These problems make it desirable to find other analytical methods. One such method is flame photometry.

Substances that are burned in a very hot flame vaporize to the atomic state. Because of the high temperatures, many of these atoms are in an excited state. When an atom returns to the ground state, light of wave-length characteristic of that particular atom is emitted. Flame photometry is based upon the collection of this

emitted light. The light can be detected by a phototube or photomultiplier tube. Isolation of a particular wavelength is achieved by placing an interference filter or diffraction grating between the flame and the light detector[4].

When sulfur oxides are burned in a hydrogen flame, the sulfur is reduced to S_2. S_2 emitts light in the region of 2500 to 4000 angstroms. By isolating the 3100 to 3300 angstrom region, interferences from OH, CN, C_2 and other impurities are excluded[5].

Construction

A schematic of the instrument is shown in Figure 26. Holes were drilled in the metal enclosure box as needed to accomodate the electrical wiring.

A surgical needle was used as the burner tip. The needle was silver soldered ro a piece of 1/8 inch stainless steel tubing which was placed in a union tee.

The hydrogen was supplied from a cylinder of Air Products zero grade hydrogen. The cylinder was connected through a flowmeter and needle valve to one side of the tee. The air-sulfur oxide mixture is drawn from the process by a Metal Bellows Co. blower through a needle valve and flowmeter to the other side of the tee. The surgical needle fits through a hole in the bottom of the enclosure and is held in place by a rubber stopper.

A 1 1/2 inch O. D. pyrex tube about 2 feet long was used to shield the flame. A bunsen burner air regulator was attached to the bottom of the tube to allow some air convection so that the flame would burn properly. The tube fit through a hole in the top of the enclosure and snugly over the rubber stopper on the bottom of the enclosure. That part of the tube that extended out of the enclosure (about 1 foot) was wrapped with asbestos and teflon tape so that the enclosure could be maintained in a light tight state.

The optical system consisted of two lenses, an interference filter and a photomultiplier tube. One lens was placed about 5 inches from the flame to collimate the light before it passed through the interference filter. The interference filter was placed immediately after this lens and was followed by the second lens. The second lens focused the light on to the window of the photomultiplier tube.

The photomultiplier tube was powered by a Hewlett Packard 6515A DC Power Supply. The current from the photomultiplier tube anode passes to an operational amplifier that is in a current follower with gain configuration. A voltage that is proportional to the anode current is sent from the output of the operational amplifier to a voltmeter. A schematic of the electrical system is

shown in Figure 27.

Operation

To begin operation, hydrogen and air flows are started and the flame lit. The pyrex shield is placed over the flame and glass wool is placed around the opening where the shield sticks out of the enclosure in order to maintain a light tight environment in the enclosure. Tape is placed around the top edges of the box to prevent light from entering the enclosure. Once the enclosure is absolutely light tight the power supply for the photomultiplier tube can be turned on. The instrument should be allowed to warm up for at least one hour. Operation can take place at any combination of gas flows, as long as a flame is maintained, and photomultiplier tube voltage, although each given set of operating conditions requires its own calibration curve.

Calibration

Calibration of the sulfur oxide detector was done by metering a known amount of SO_2 through a flowmeter into a known amount of air. A hydrogen flow rate of about 800 ml/min (31 on a Gilmont flowmeter H554) and an air-SO_2 rate of 500 ml/min (32 on Gilmont flowmeter H438) seemed to provide the most sensitivity, so those flows were used for calibration. The photomultiplier tube was maintained at a

potential of 900 volts. The calibration data is shown in Table 5 and a calibration curve in Figure 28.

The calibration data show that the detector is not as sensitive or accurate as might be expected. The minimum concentration that could be detected was about 900 ppm and and a concentration could be resolved only to about ±100 ppm. The capabilities of the detector might be improved with some changes in the amplification system and voltmeter. One possibility is to use an anti-logarithmic amplifier to expand the scale of the output for a given input.

Electrical Resistivity of a Bed of Spherical Glass Beads

It has long been recognized that flyash electrical resistivity, and thus flyash electrostatic precipitation efficiency, varies widely with flue gas composition and constituent concentration. Recently Ditl and Coughlin developed a model based on "the capillary condensation of liquid at the contact points of ash particles" to explain this phenomenon[6]. The model accounts for the effects of temperature, flue gas moisture content, and the concentration of any conditioning agent present in the flue gas on the flyash resistivity. A simple experiment using spherical glass beads to test the validity of this model is reported here.

Apparatus

A schematic of the apparatus is shown in Figure 29. The heart of the apparatus was a point-plane electrode system. The plane was a disk 3.81 cm in diameter upon which the glass beads were packed to form a bed. The needle point sits about 1 1/4 inches above the plane and was connected to a Spellman High Voltage Power Supply. The electrode system was contained in a one quart juice can. Holes drilled in the side of the can allowed for the introduction of am air stream to the can. The humidity

of this air stream was controlled either by passing the air through a bed of Drierite (for dry air) or by bubbling the air through a flask of water of controlled temperature. This gas stream was heated by a bunsen burner before entering the can. The can was wrapped with heating tape to control the temperature of the glass bead bed. The temperature inside the can was measured with a thermometer. Current flowing through the glass bead bed was measured with a Keithley Electrometer Model 610C.

Experimental

Glass beads of a given mean diameter were packed into a bed on the lower electrode. Dry air, made by passing laboratory air through an impinger filled with Drierite, at room temperature was passed through the can for about one hour so that the system could equilibrate. Then the temperature in the can was raised in small steps. At each temperature the system was allowed to equilibrate before the current being passed through the bed was measured. In each case the applied voltage was 10 KV. This procedure was followed until a maximum temperature of 160 C was attained. At this point the system was allowed to cool back to room temperature. After the system was cool, leaving the bed of glass beads undisturbed, air of the

desired humidity was introduced to the container. After allowing some time for equilibration, the same procedure of raising the temperature and measuring the current was followed. The entire procedure was repeated for beds of varying bead size.

Results and Discussion

The data obtained is presented in Table 6. Graphs of log resistivity versus temperature for various mean bead diameters are shown in Figures 30-33. According to the proposed model, the electrical conductivity is given by

$$K=K_V+K_S\cdot\emptyset$$

where $\emptyset=\ln\left(\frac{\ln(p/p_0)min}{\ln(p_k/p_0)}\right)$ and $K_S=k/(d_p\cdot\rho_S\cdot\tan\alpha)$.

Theoretical curves were generated by the method shown in Figure 34. The theoretical curve for each mean bead diameter is included in the graphs shown in Figures 30-33. Clearly the theoretical and experimental curves are very different.

One major problem in this analysis is the determination of the dry bead resistivity line. The curve of log resistivity versus temperature for dry glass beads should be linear. The curves for dry beads in Figures 30-33 are clearly nonlinear, although in some cases the curve could be approximated by two straight lines. The nonlinearity of the experimental dry bead curves, however, causes some

problems in the use of the model. Not only is it difficult to determine the exact intersection point of the dry and humid curves, but the true values of the dry curve are impossible to determine accurately.

An attempt was made to extrapolate dry curves from the data for the humid curves. The data generated using this extrapolation is shown in Table 7. Figures 35-38 show the new theoretical curves and experimental curves for the humid air. Agreement between the predicted and experimental curves appears to be better for the case using the extrapolated dry bead resistivity curve than for the case using the experimental dry bead data. Of special note is the fact that the dependence of resistivity maxima on mean bead size is predicted by the model for the smallest three bead sizes, even though the exact location of the maxima are not. These results suggest that the model does describe, at least to some extent, the mechanism involved in the electrical conduction process in layers of spherical particles.

Appendix

Appendix A

ble 1: Experimental Conditions of Alternative Flyash Conditioning Agent Study

Solution	Solution Feed Rate ml/min	Gas Rate ft^3/min	Temperature at Solution Injection °C	Temperature Flyash °C
0 M NaCl	4.1	45	600	185
5 M $CaCl_2$	4.1	43	605	190
ak Ammonia Liquor	16	44	645	195
SO_4 Waste	18	51	555	178
t Scrubber Underflow	26.5	49	525	185
0 M lfamic Acid	60	50	540	195

ble 2: Peaks Observed with Energy Dispersive X-Ray Detector Used in Conjunction with a SEM

Peak (ev)	Corresponding Element
1.475	Al
1.750	Si
3.325	K_K
3.625	K_K
4.525	Ti_K
4.930	Ti_K
6.400	Fe_K
7.060	Fe_K
2.300	S*

*Observed only on SO_3 treated samples.

Table 1: Experimental Conditions of Alternative Flyash Conditioning Agent Study

Solution	Solution Feed Rate ml/min	Gas Rate ft^3/min	Temperature at Solution Injection °C	Temperature Flyash °C
.50 M NaCl	4.1	45	600	185
.25 M $CaCl_2$	4.1	43	605	190
Weak Ammonia Liquor	16	44	645	195
$PbSO_4$ Waste	18	51	555	178
Wet Scrubber Underflow	26.5	49	525	185
.50 M Sulfamic Acid	60	50	540	195

Table 2: Peaks Observed with Energy Dispersive X-Ray Detector Used in Conjunction with a SEM

Peak (ev)	Corresponding Element
1.475	Al
1.750	Si
3.325	K_K
3.625	K_K
4.525	Ti_K
4.930	Ti_K
6.400	Fe_K
7.060	Fe_K
2.300	S*

*Observed only on SO_3 treated samples.

Table 3: Electron Microprobe X-Ray Counts for Unconditioned Flyash

Fe	S	Na	Fe	S	Na
Background			Standard		
719	349	399	19404	46482	253
708	386	375	19715	46481	244
740	379	421	19373	46266	215
			19132	46028	223
			19560	46504	234
Particle 1 Across			Particle 1 Down		
345	56	291	6119	136	558
617	61	1035	4204	70	373
1718	87	636	4410	91	509
28737	147	530	575	85	347
282	49	252	1522	54	265
150	39	137	21630	183	829
57	36	124	1841	86	551
			268	60	411
Particle 2 Across			Particle 2 Down		
58866	171	245	58947	143	225
56762	168	309	57198	157	235
55331	151	385	55481	132	224
59079	141	240	54285	145	254
57794	129	288	57821	185	314
57233	123	254	56106	244	370
52484	145	384	58072	159	317
Particle 3 Across			Particle 3 Down		
1075	109	626	2770	105	846
1293	95	1000	1712	242	1747
149	73	174	1140	87	761
1372	86	689	951	120	1403
2645	45	530	1478	89	708
988	113	804	1466	98	937
861	104	776	427	43	226
854	133	1109			
701	121	1370			

Table 3: Continued

Fe	S	Na	Fe	S	Na
Particle 4 Across			Particle 4 Down		
651	60	436	529	74	464
156	66	287	335	89	491
313	110	558	195	101	337
256	83	517	383	112	484
601	102	734	237	95	440
219	100	406			
Particle 5 Across			Particle 5 Down		
2881	135	791	389	79	286
1250	165	619	4254	84	959
2195	128	1019	1432	254	1740
4903	154	748	2363	98	561
5244	118	562	2092	106	814
			2033	95	921
Particle 6 Across			Particle 6 Down		
231	287	969	2052	1325	686
197	100	360	475	16235	693
1780	354	1029	594	1991	550
557	11062	442	341	216	674
Particle 7 Across					
1273	81	684			
1575	93	680			
1873	78	737			
1306	77	874			
1548	73	1214			
767	104	1087			
1924	107	1120			
1553	82	710			
664	57	241			
1193	63	98			
1952	73	886			
1220	77	493			
1989	77	753			
1249	65	599			

Table 4: Electron Microprobe X-Ray Counts for SO_3 Treated Flyash

Fe	S	Na	Fe	S	Na
	Background			Standard	
719	349	399	19464	46482	253
708	386	375	19715	46481	244
740	379	421	19373	46266	215
			19132	46028	223
			19560	46504	234
	Particle 1 Across			Particle 1 Down	
13162	91	152	14733	91	186
4494	59	15	16097	96	154
3020	53	106	16037	94	143
11879	142	157	17112	81	159
15665	100	172	17797	119	192
16456	104	169	26551	193	239
17721	135	185	42269	268	201
16687	111	208	17572	130	369
15932	126	321	16852	124	240
15806	81	223	14380	109	95
15095	85	195	16361	104	203
14583	96	188	15599	92	252
14643	107	182	15227	89	318
15327	98	140	14628	106	282
12588	84	158	14341	81	218
14598	82	146			
	Particle 2 Across			Particle 2 Down	
445	87	334	370	60	417
357	76	320	400	61	249
434	62	275	367	84	325
366	68	356	455	82	342
328	58	325	422	64	299
502	77	367	373	97	228
419	78	419			
394	87	336			

Table 4: Continued

Fe	S	Na	Fe	S	Na
Particle 3 Across			Particle 3 Down		
819	95	266	681	64	238
594	81	474	617	76	293
458	74	410	436	71	221
481	49	199	514	69	381
407	71	347	342	78	329
			515	84	503
Particle 4 Across			Particle 4 Down		
2541	65	326	1513	79	482
3241	80	752	1337	66	521
3558	73	470	946	69	276
2828	77	313	2164	82	618
1100	178	172	2015	77	470
4438	106	428	2473	1325	438
2364	71	556	3405	58	297
			801	69	388
			1474	91	487
			857	78	443
			3916	83	504
Particle 5 Across			Particle 5 Down		
956	83	500	1082	73	329
1689	76	666	1281	94	389
1581	103	675	1187	77	280
382	102	431	891	97	366
1277	74	458	1195	69	380
1223	121	554	1046	79	443
1005	75	518			
856	114	477			
401	79	275			
1444	88	593			

Table 4: Continued

Fe	S	Na	Fe	S	Na
Particle 6 Across			Particle 6 Down		
1360	101	366	1125	73	546
1533	85	342	2275	86	477
1231	76	451	1643	81	544
1440	71	415	1405	79	699
912	83	414	1529	66	442
			777	89	646
			1714	67	638
Particle 7 Down					
125	92	119			
529	92	137			
1608	88	866			
1166	85	722			
1706	70	518			
1906	72	589			
736	64	635			
2065	86	753			
Particle 8 Across			Particle 8 Down		
725	98	380	672	86	470
1443	102	472	509	57	386
737	59	378	1043	119	419
925	40	83	717	81	518
1174	103	434	1002	69	419
Particle 9 Across			Particle 9 Down		
53	40	70	1602	70	426
59	33	60	437	84	163
60	43	90	1729	170	376
2108	129	59	1339	104	554
2872	75	639	42889	131	286
959	249	252	543	139	387
2255	749	465	2150	93	417
1801	412	374	872	73	356
			860	218	195
			262	104	106

Table 4: Continued

Fe	S	Na	Fe	S	Na
Particle 10 Across			Particle 10 Down		
328	68	132	686	116	708
370	131	485	398	178	589
757	251	496	453	141	455
465	65	323	670	83	608
1999	199	375	701	96	686
			3127	390	707
			1562	137	432

Table 5: Calibration Data for Sulfur Oxide Detector

SO_2 Flow (ml/min)	Air Flow (ml/min)	ppm SO_2 in Gas Mixture	Readout * Voltage (V)
0	39500	0	0.875
36.1	39500	910	0.880
49.3	39500	1250	0.892
59.2	39500	1500	0.899
68.5	39500	1730	0.905
79.0	39500	2000	0.911
87.3	39500	2200	0.919
94.2	39500	2380	0.925
104.8	39500	2650	0.933
116.0	39500	2930	0.941
116.0	38500	2980	0.945
116.0	35200	3280	0.950
116.0	31200	3730	0.960
116.0	27400	4260	0.980
116.0	22900	5040	1.00
116.0	18800	6130	1.03
116.0	14800	7380	1.07
116.0	11750	10670	1.15

* H_2 flow- flowmeter reading of 31 on Gilmont flowmeter H554
Air-SO_2 flow- flowmeter reading of 32 on Gilmont flowmeter H438
Photomultiplier tube voltage- 900V

Table 6: Resistivity as a Function of Temperature for a Bed of Glass Beads

$d_{p_{av}}$=387 microns l=0.4 cm d_{bed}=3.81 cm

T(°C)	i(Amps) ($x10^7$)	ρ (Ω-cm) ($x10^{-9}$)
	Dry	
26	6.0	475.0
32	8.9	320.0
48	14.0	204.0
76	27.0	106.0
111	95.5	29.8
158	300.0	9.5
186	440.0	6.5
	Humidified C_v=4.5%	
30	165.0	17.3
33	230.0	12.4
35	250.0	11.4
36	255.0	11.2
42	265.0	10.7
46	249.0	11.4
52	270.0	10.5
60	195.0	14.6
64	160.0	17.8
72	78.0	36.5
83	63.5	44.9
90	62.0	46.0

Table 6: Continued

T(°C)	i(Amps) ($x10^7$)	ρ (Ω-cm) ($x10^{-9}$)
94	67.5	42.2
108	75.0	38.0
115	90.0	31.7
133	125.0	22.8
156	225.0	12.7

$d_{p_{av}}$=460 microns l=0.4 cm d_{bed}=3.81 cm

Dry

29	14.8	192.0
31	15.2	188.0
37	18.0	158.0
44	23.5	121.0
52	33.5	85.1
66	53.5	53.3
76	73.0	39.0
89	101.0	28.2
98	100.0	28.5
111	114.0	25.0
125	136.0	21.0
135	187.0	15.2
146	242.0	11.8

Humidified C_v=4.05%

33	285.0	10.0
35	290.0	9.8

Table 6: Continued

T(°C)	i(Amps) ($x10^7$)	ρ (Ω-cm) ($x10^{-9}$)
36	294.0	9.7
40	299.0	9.5
47	300.0	9.5
53	252.0	11.3
60	188.0	15.2
67	115.0	24.8
75	88.5	32.2
85	87.5	32.6
91	91.0	31.3
101	107.0	26.6
107	116.0	24.6
121	150.0	19.0
131	188.0	15.2
137	220.0	13.0
154	318.0	8.96

$d_{p_{av}}$=545 microns l=0.4 cm d_{bed}=3.81 cm

Dry

26	17.0	150.0
34	21.0	136.0
38	27.5	104.0
48	37.0	77.0
59	62.0	46.0

Table 6: Continued

T(°C)	i(Amps) ($x10^7$)	ρ(Ω-cm) ($x10^{-9}$)
65	78.5	36.3
72	107.0	26.0
83	125.0	22.8
89	130.0	21.9
96	130.0	21.9
102	133.0	21.4
112	155.0	18.1
124	180.0	16.0
132	195.0	14.5
144	235.0	12.1
140	290.0	10.1
160	350.0	8.4
	Humidified	C_v=4.0%
32	280.0	10.2
33	300.0	9.5
37	302.0	9.4
41	310.0	9.2
47	309.0	9.2
54	239.0	11.9
62	122.0	23.4
68	106.0	26.9
72	108.0	26.4
79	110.0	25.9

Table 6: Continued

T(°C)	i(Amps) ($x10^7$)	ρ (Ω-cm) ($x10^{-9}$)
87	120.0	23.8
98	140.0	20.4
104	150.0	19.0
114	162.0	17.6
123	179.0	15.9
130	192.0	14.8
140	231.0	12.3
155	285.0	10.0

$d_{p_{av}}$=650 microns l=0.4 cm d_{bed}=3.81 cm

Dry

26	11.7	244.0
28	12.2	234.0
33	14.7	194.0
38	17.6	162.0
47	27.7	103.0
54	39.8	71.6
57	48.8	58.4
65	66.5	42.8
72	79.5	35.8
80	92.0	31.0
89	120.0	23.7
104	102.0	27.9

Table 6: Continued

T(°C)	i(Amps) ($x10^7$)	ρ(Ω-cm) ($x10^{-9}$)
110	113.0	25.2
123	139.0	20.5
135	200.0	14.2
144	269.0	10.6
148	295.0	9.7
	Humidified	C_v=4.0%
28	340.0	8.4
30	349.0	8.2
36	332.0	8.6
42	329.0	8.7
49	332.0	8.6
53	320.0	8.9
58	224.0	12.7
62	178.0	16.0
64	132.0	21.6
72	108.0	26.4
76	102.0	27.9
80	101.0	28.2
82	103.0	27.7
86	109.0	26.1
88	114.0	25.0
94	124.0	23.0
106	160.0	17.8
124	215.0	13.2

Table 7: Resistivity Versus Temperature Data Generated Using the Model of Ditl and Coughlin

T (°C)	p_o (psi)	ϕ	$K_s\phi$ (1/Ω-cm) (x10^{12})	K_v (1/Ω-cm) (x10^{12})	K (1/Ω-cm) (x10^{11})	ρ (Ω-cm) (x10^{-10})
$d_{p_{av}}$=387 microns T_{int}=116°C ϕ=1.33 K_s=4.40x10^{-12}						
55	2.284	2.93	12.9	6.8	1.97	5.08
60	2.889	2.46	10.8	7.7	1.85	5.40
65	3.628	2.14	9.4	8.7	1.81	5.53
68	4.143	1.98	8.7	9.3	1.81	5.54
70	4.520	1.89	8.3	9.8	1.81	5.52
75	5.592	1.70	7.5	11.1	1.86	5.37
80	6.869	1.56	6.8	12.6	1.94	5.15
$d_{p_{av}}$=460 microns T_{int}=117°C ϕ=1.54 K_s=6.6x10^{-12}						
40	1.070	6.42	42.3	8.2	5.05	1.98
45	1.390	4.44	29.2	9.3	3.85	2.60
50	1.789	3.42	22.5	10.4	3.29	3.04
55	2.284	2.80	18.4	11.6	3.00	3.33
60	2.889	2.38	15.7	13.0	2.87	3.49
63	3.315	2.19	14.4	13.9	2.83	3.53
65	3.628	2.08	13.7	14.5	2.82	3.54
68	4.143	1.94	12.8	15.6	2.84	3.52
70	4.520	1.85	12.2	16.4	2.86	3.50
75	5.592	1.68	11.0	18.3	2.94	3.40
80	6.869	1.54	10.1	20.6	3.07	3.25
$d_{p_{av}}$=545 microns T_{int}=90°C ϕ=1.43 K_s=2.5x10^{-12}						
40	1.070	4.78	12.0	22.7	3.47	2.88
45	1.390	3.32	8.3	24.1	3.24	3.09
50	1.789	2.57	6.4	25.8	3.22	3.11
55	2.284	2.10	5.3	27.4	3.27	3.06
60	2.889	1.79	4.5	29.2	3.37	2.96

Table 7: Continued

T	p_o	ϕ	$K_s\phi$	K_v	K	ρ
$d_{p_{av}}$=650 microns		T_{int}=86 °C		ϕ=1.12	K_s=1.96x10^{-12}	
40	1.070	4.53	8.8	15.6	2.45	4.08
45	1.390	3.14	6.2	17.2	2.34	4.27
50	1.789	2.43	4.8	18.9	2.36	4.23
55	2.284	1.99	3.9	20.8	2.47	4.09
60	2.889	1.69	3.3	22.9	2.96	3.38

Appendix B

Figure Captions

Figure 1: Schematic diagram of apparatus for testing flyash conditioning agents.

Figure 2: Plot of flyash resistivity versus time with NaCl, $CaCl_2$ and ammonia liquor as conditioning agents.

Figure 3: Plot of flyash resistivity versus time with $PbSO_4$ waste and wet scrubber underflow as conditioning agents.

Figure 4: Plot of flyash resistivity versus time with sulfamic acid as the conditioning agent.

Figure 5: Plot of flyash resistivity versus time with SO_3 as the conditioning agent.

Figure 6: Flyash polished for electron microprobe analysis. Magnification 160X.

Figure 7: SEM photograph of dry sieved flyash. Size fraction 53 to 105 microns. Magnification 1600X.

Figure 8: SEM photograph of dry sieved flyash. Size fraction 53 to 105 microns. Magnification 1600X.

Figure 9: SEM photograph of dry sieved flyash. Size fraction 53 to 105 microns. Magnification 1600X.

Figure 10: SEM photograph of wet sieved flyash. Size fraction 53 to 105 microns. Magnification 840X.

Figure 11: SEM photograph of wet sieved flyash. Particle sizes of 53 to 105 microns. Magnification 880X.

Figure 12: SEM photograph of wet sieved flyash of size fraction 44 to 53 microns. Magnification 900X.

FIGURE 1.

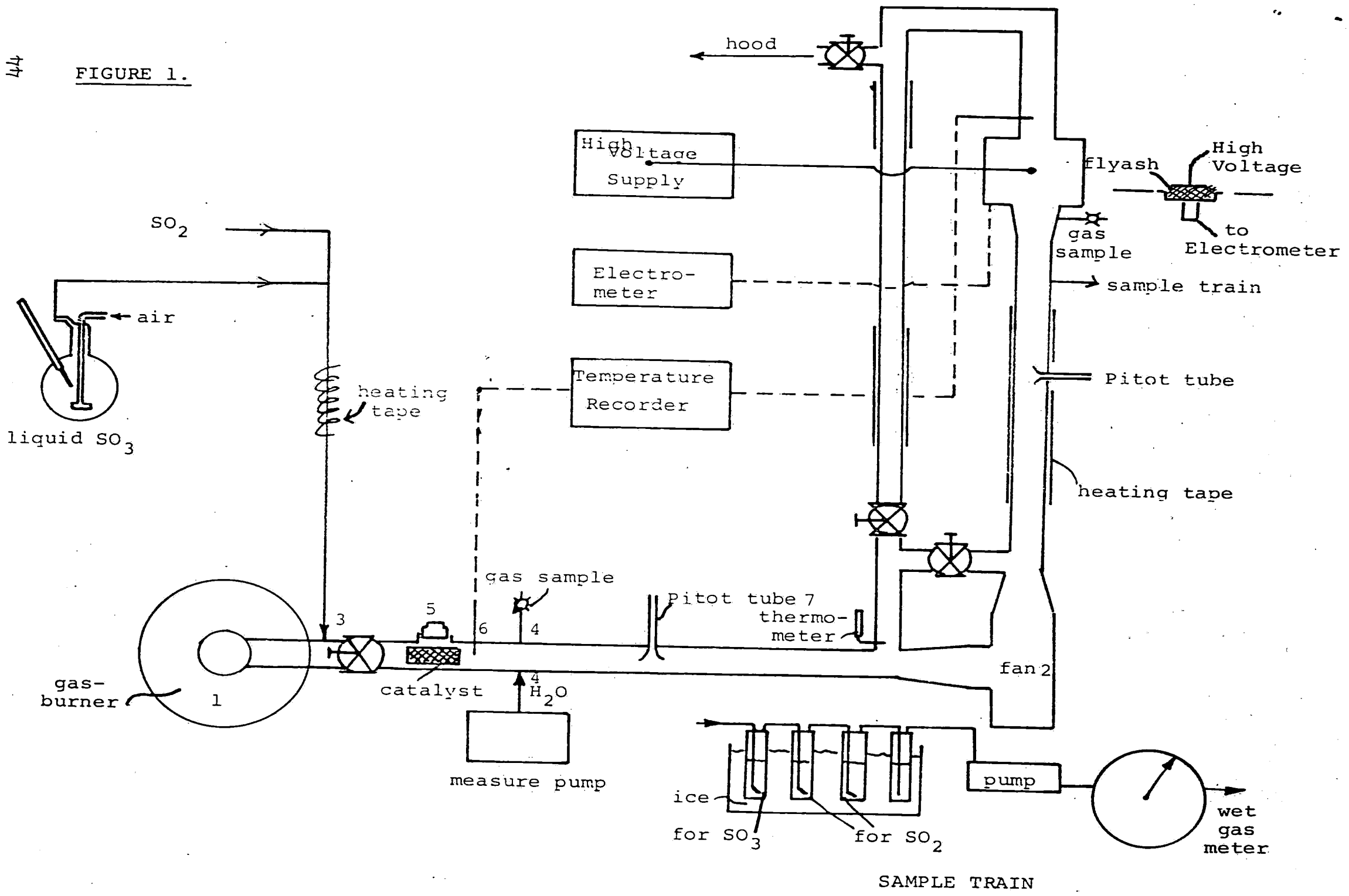

SAMPLE TRAIN

FIGURE 2

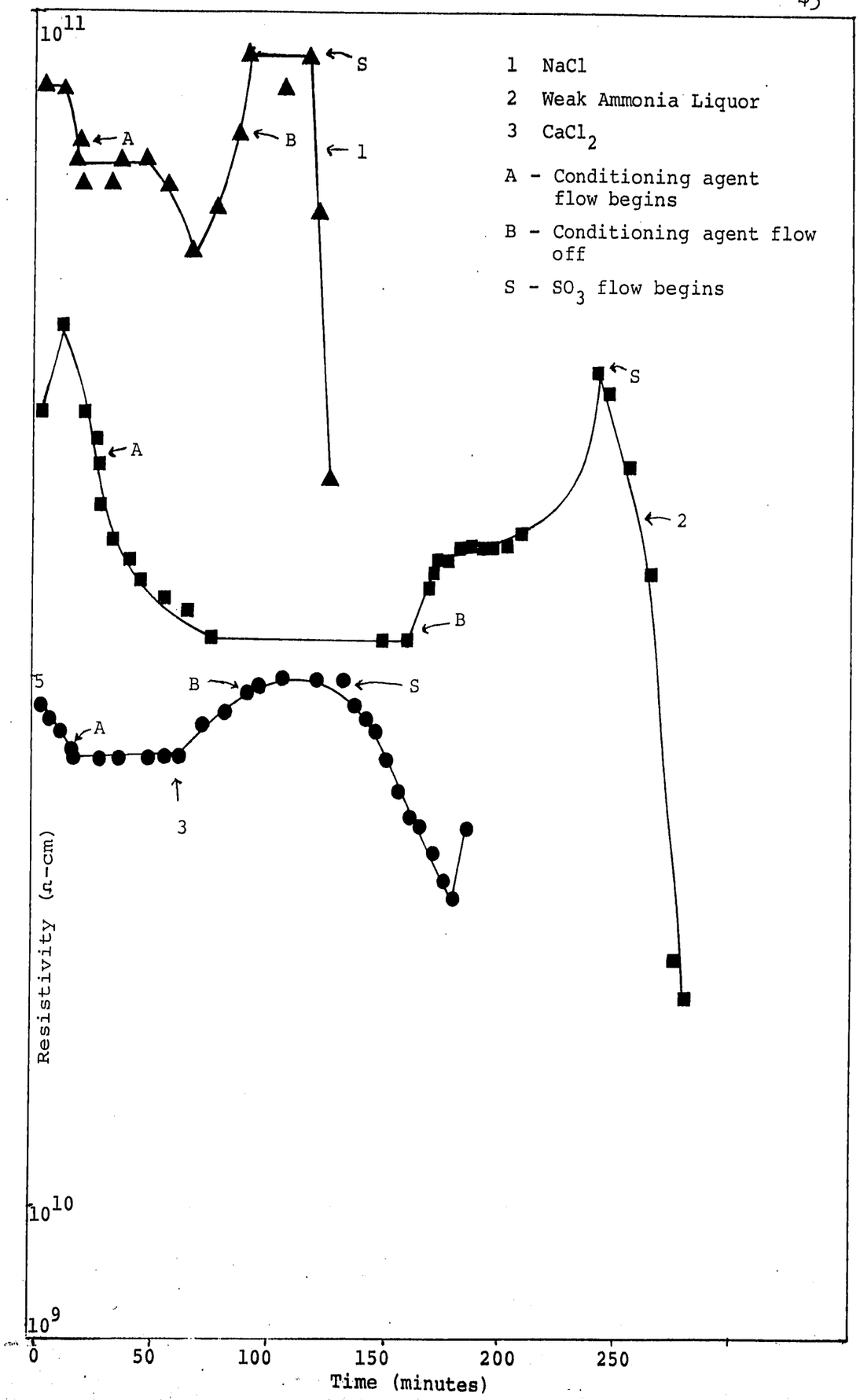
10^{11}
10^{10}
10^{9}
Resistivity (Ω-cm)
0
50
100
150
200
250
Time (minutes)
1 NaCl
2 Weak Ammonia Liquor
3 $CaCl_2$
A - Conditioning agent flow begins
B - Conditioning agent flow off
S - SO_3 flow begins
A
B
S
1
2
3

FIGURE 3

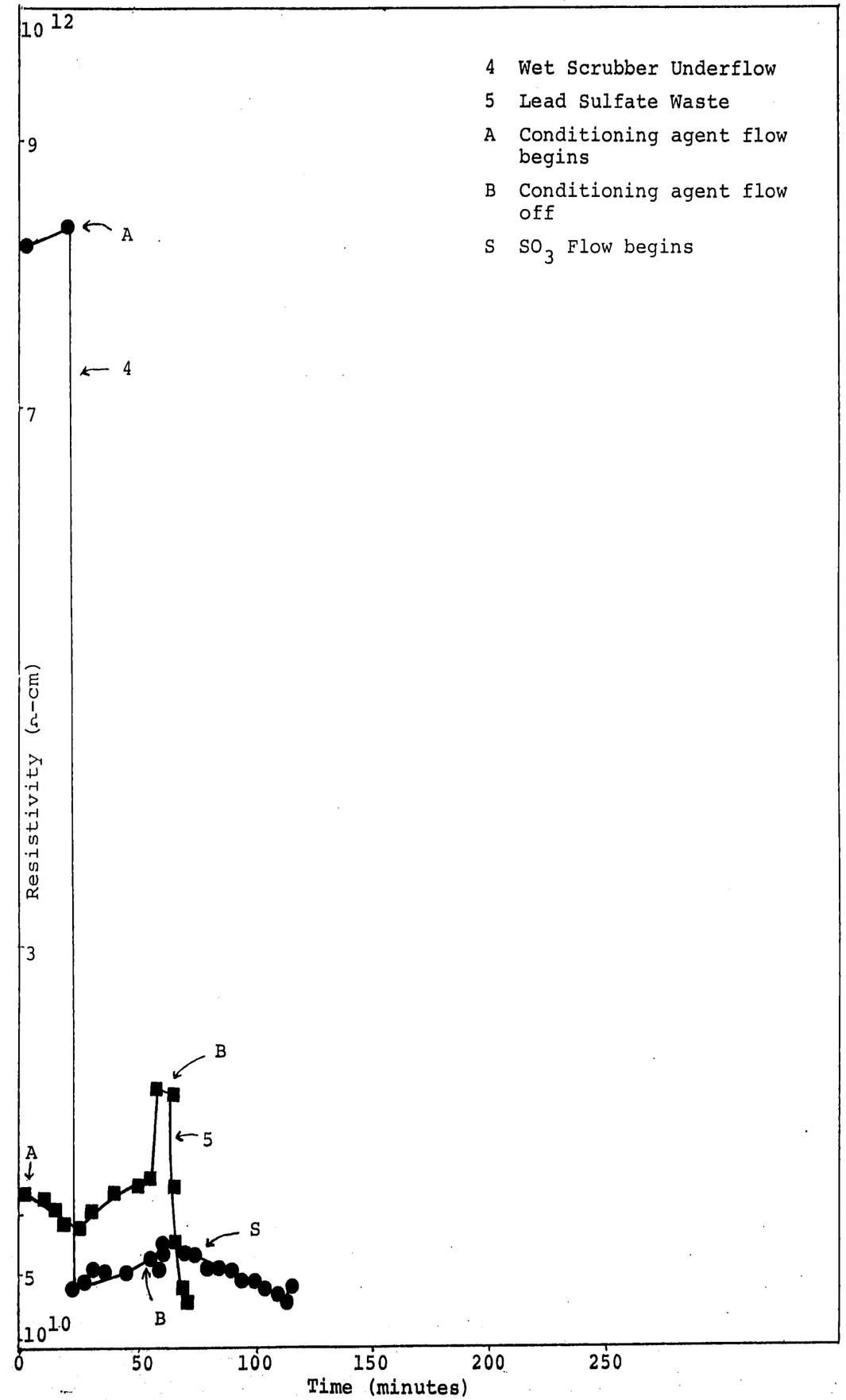
4 Wet Scrubber Underflow
5 Lead Sulfate Waste
A Conditioning agent flow begins
B Conditioning agent flow off
S SO_3 Flow begins
Resistivity (Ω-cm)
Time (minutes)
10 12
9
7
3
5
10 10
0
50
100
150
200
250
A
4
B
5
S
B
A

FIGURE 4

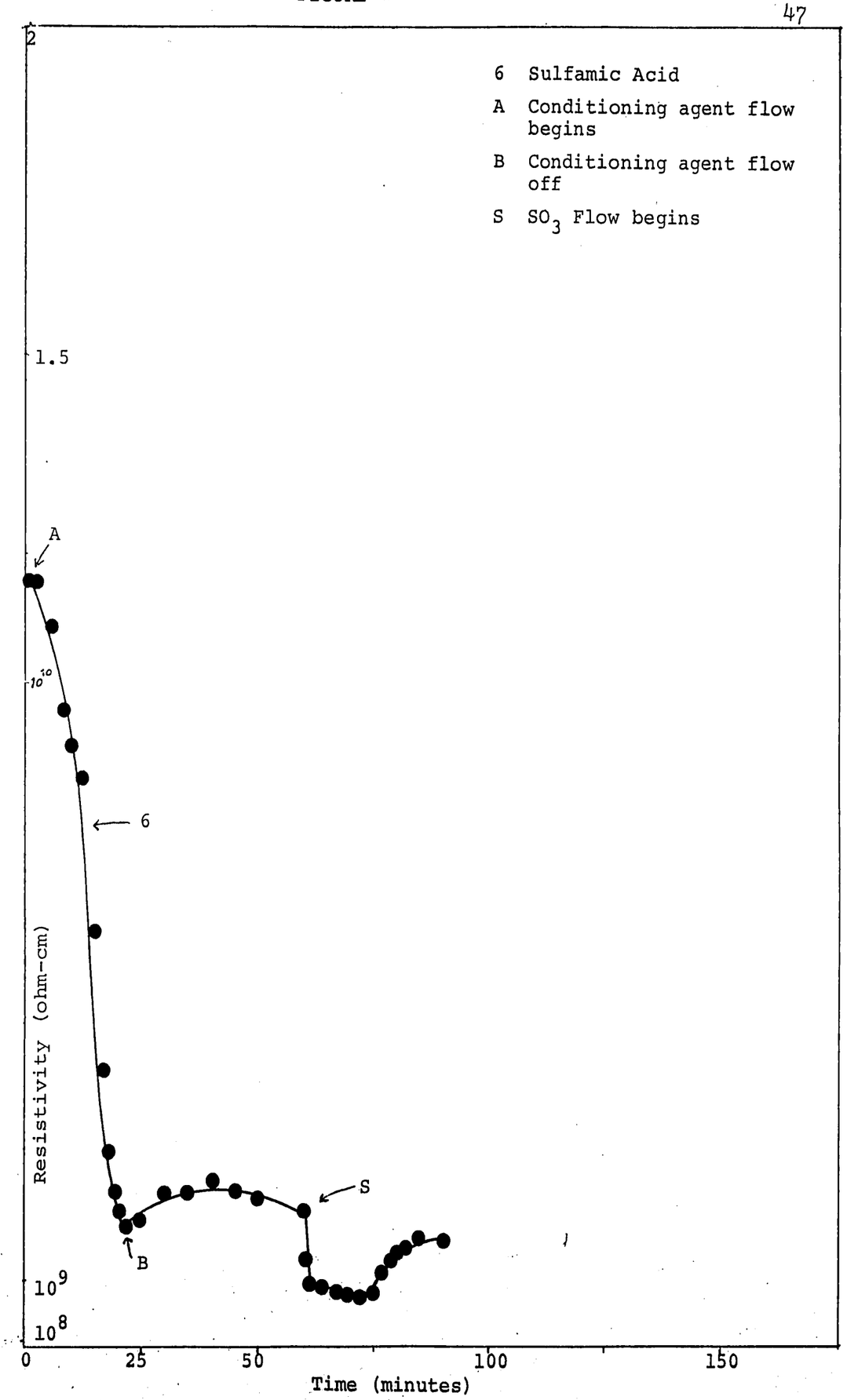
6 Sulfamic Acid
A Conditioning agent flow begins
B Conditioning agent flow off
S SO_3 Flow begins
2
1.5
10^{10}
10^9
10^8
Resistivity (ohm-cm)
A
6
B
S
0
25
50
100
150
Time (minutes)

Figure 5

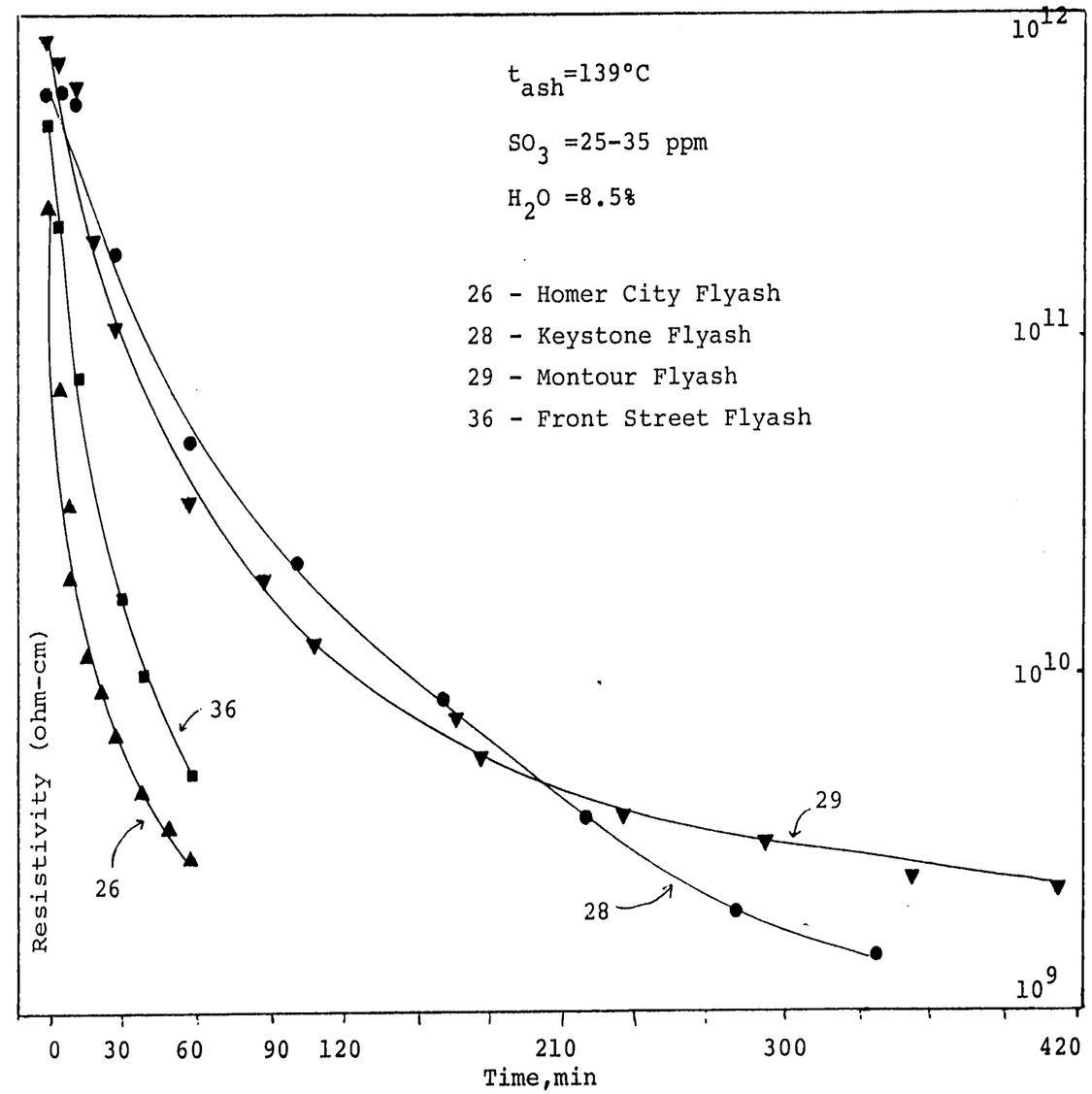
t_{ash}=139°C
SO_3 =25-35 ppm
H_2O =8.5%
26 - Homer City Flyash
28 - Keystone Flyash
29 - Montour Flyash
36 - Front Street Flyash
10^{12}
10^{11}
10^{10}
10^{9}
Resistivity (ohm-cm)
36
26
29
28
0
30
60
90
120
210
300
420
Time,min

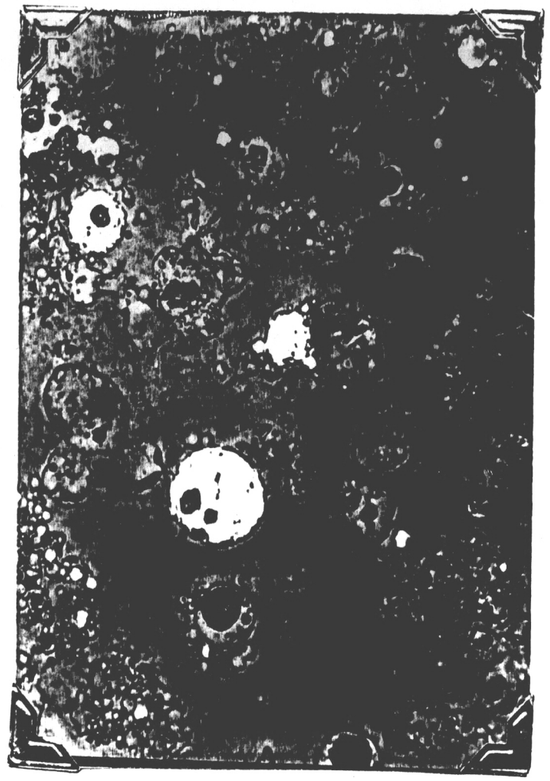

Figure 6

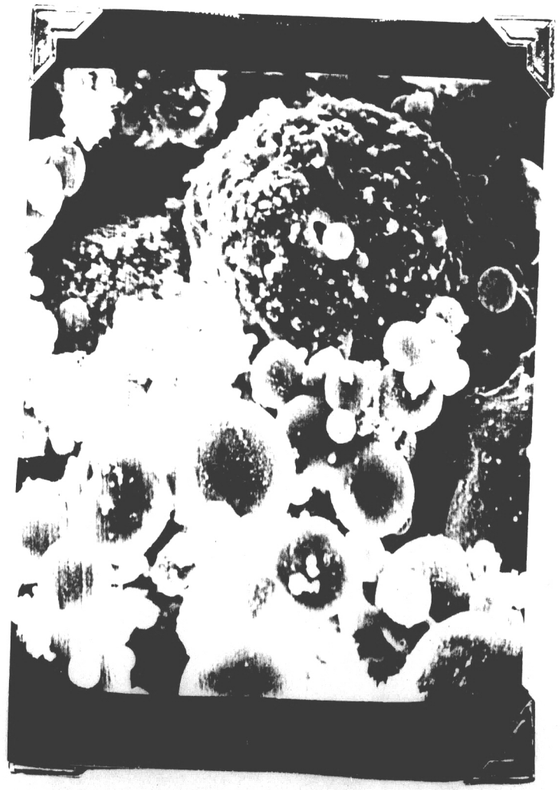

Figure 7

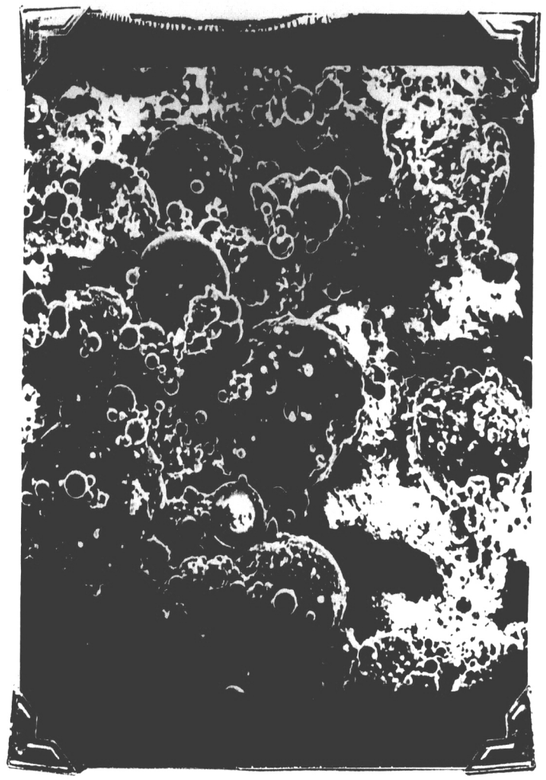

Figure 8

Figure 9

Figure 10

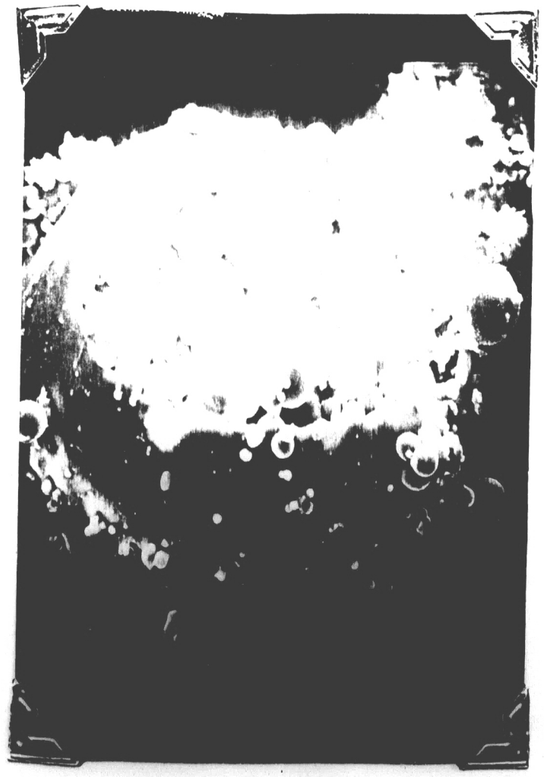

Figure 11

Figure 12

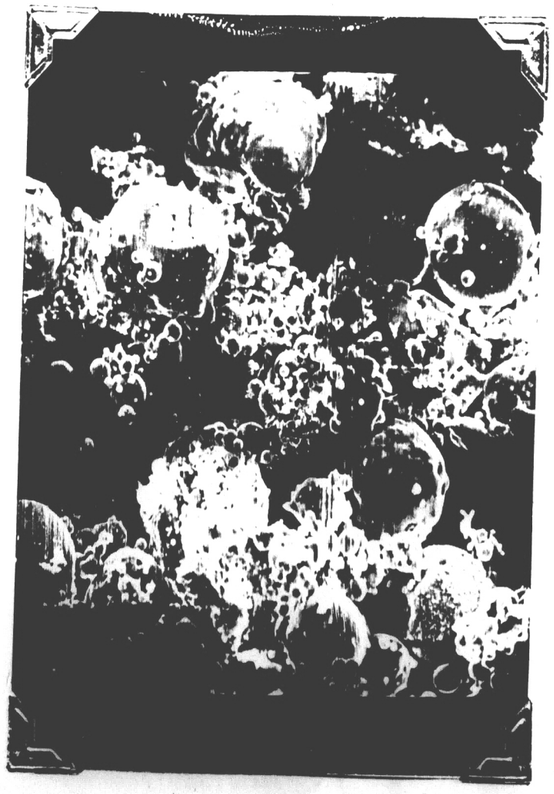

Figure 13

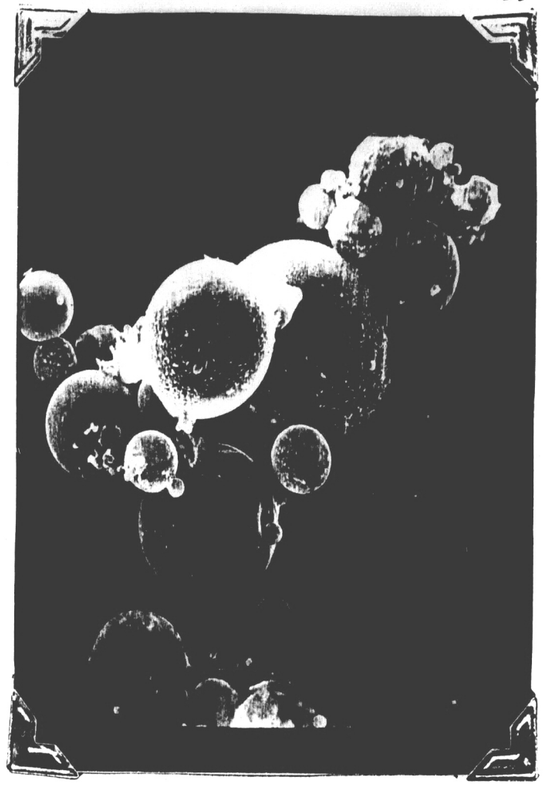

Figure 14

Figure 15

Figure 16

Figure 17

Figure 18

Figure 19

Figure 20

Figure 21

Figure 22

Figure 23

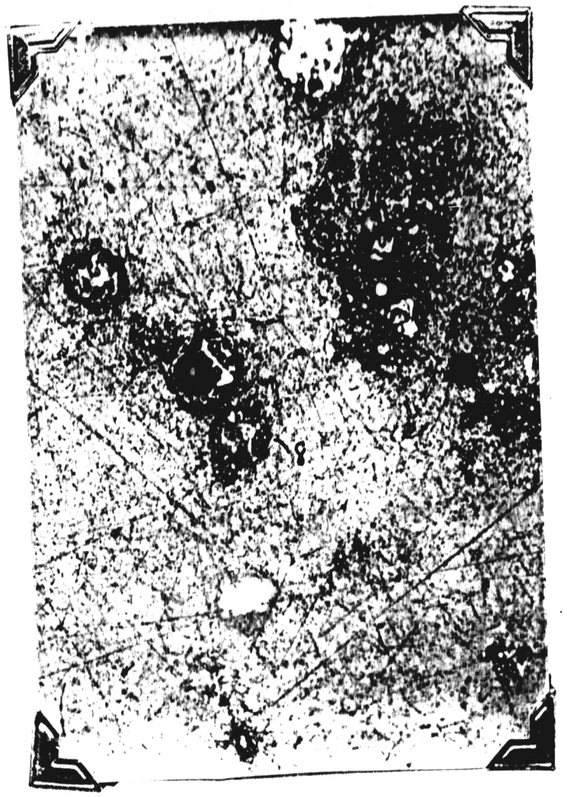

Figure 24

Figure 25

Figure 26

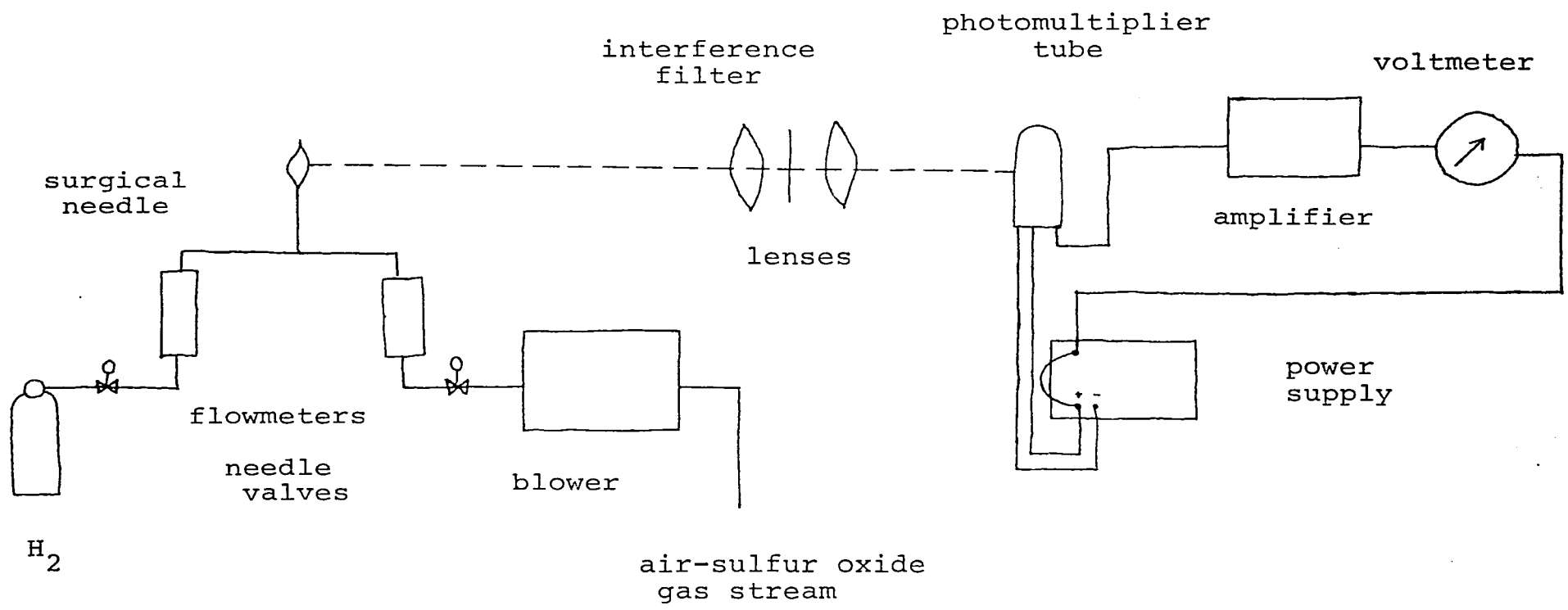
photomultiplier
tube
interference
filter
voltmeter
surgical
needle
amplifier
lenses
power
supply
flowmeters
needle
valves
blower
H_2
air-sulfur oxide
gas stream

Figure 27

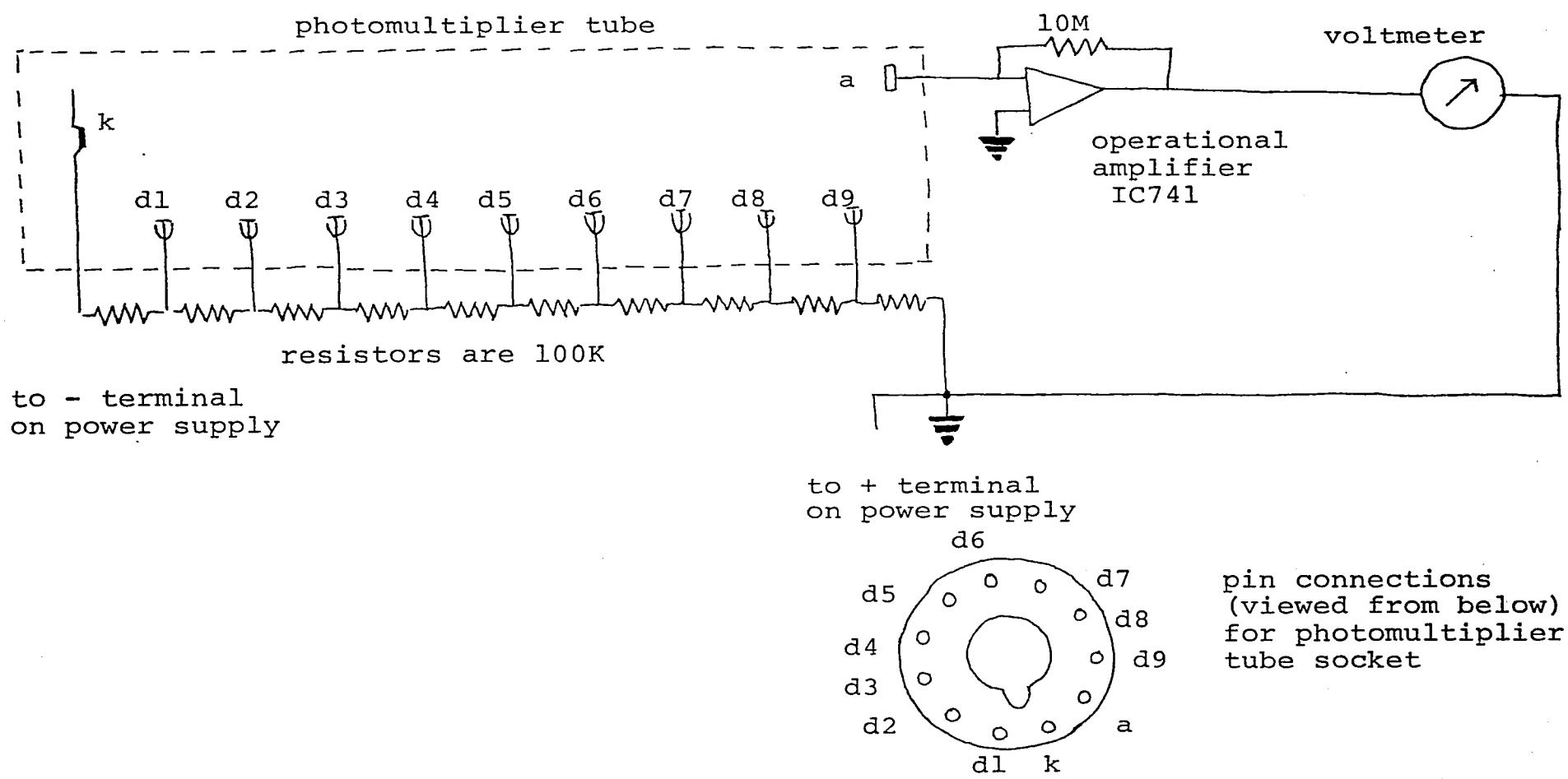
photomultiplier tube
10M
voltmeter
a
k
operational
amplifier
IC741
d1
d2
d3
d4
d5
d6
d7
d8
d9
resistors are 100K
to - terminal
on power supply
to + terminal
on power supply
d6
d5
d7
d8
d4
d9
d3
d2
a
d1
k
pin connections
(viewed from below)
for photomultiplier
tube socket

Figure 28

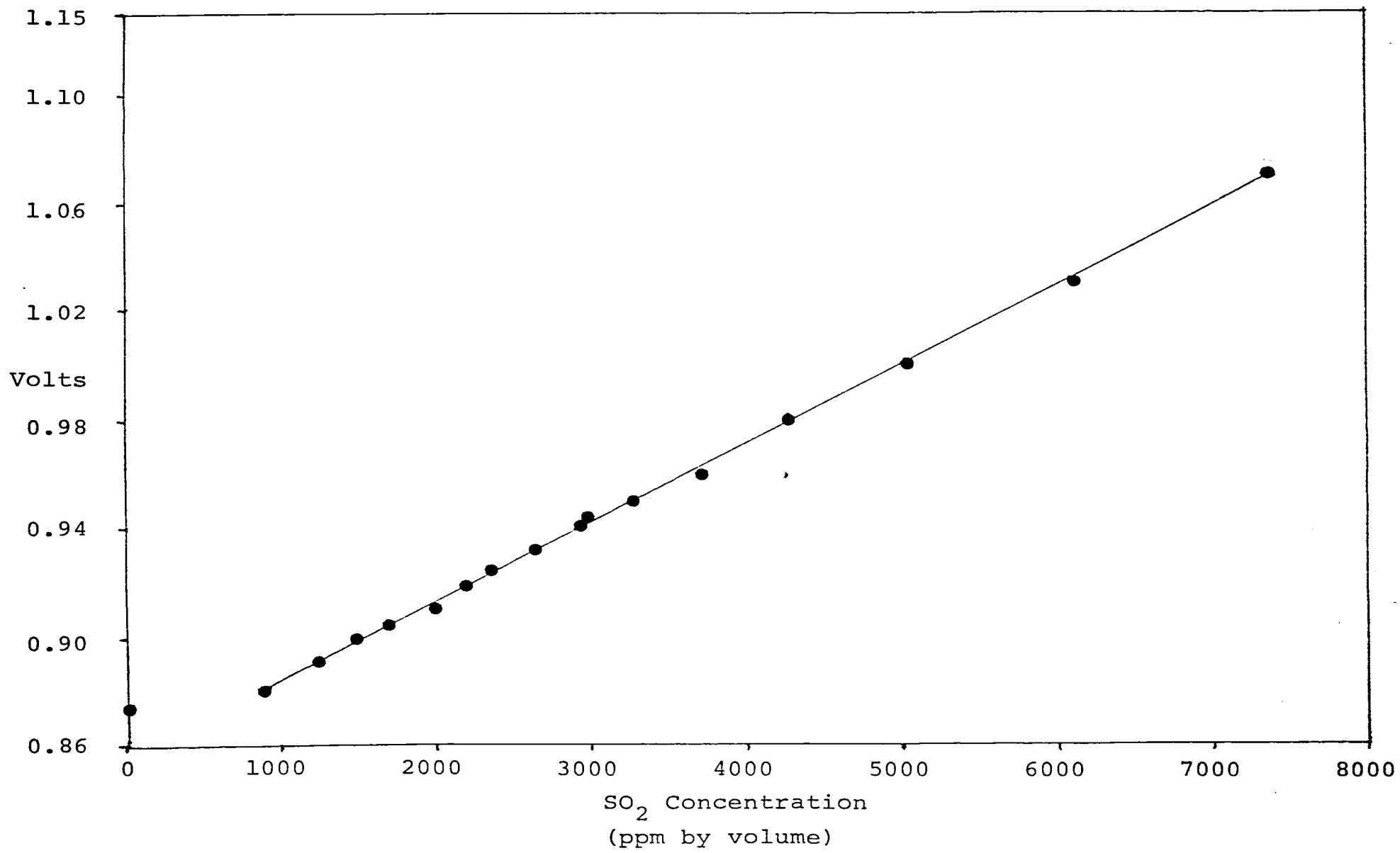
1.15
1.10
1.06
1.02
Volts
0.98
0.94
0.90
0.86
0
1000
2000
3000
4000
5000
6000
7000
8000
SO_2 Concentration
(ppm by volume)

Figure 29

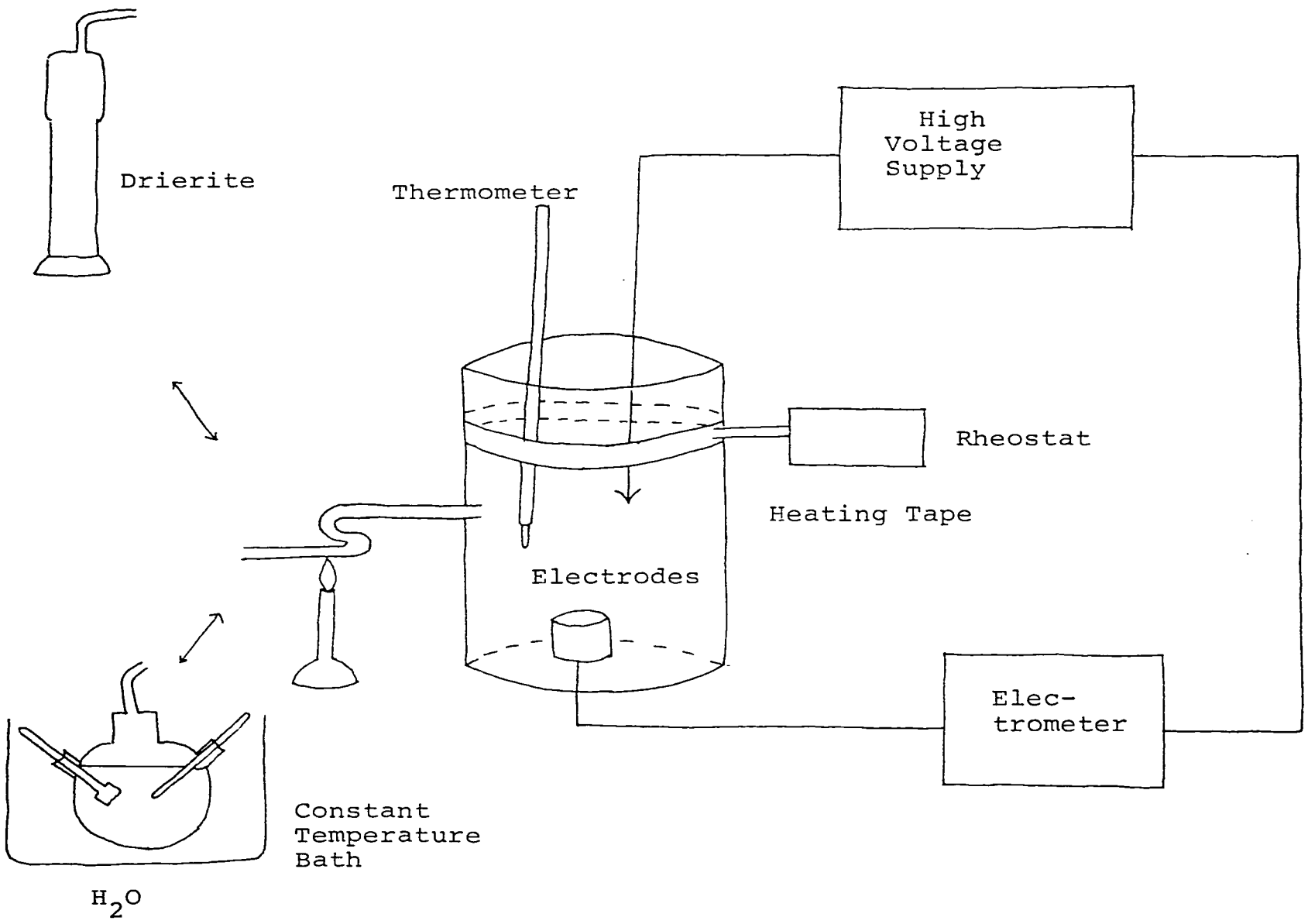
Drierite
Thermometer
High
Voltage
Supply
Rheostat
Heating Tape
Electrodes
Elec-
trometer
Constant
Temperature
Bath
H_2O

Figure 30

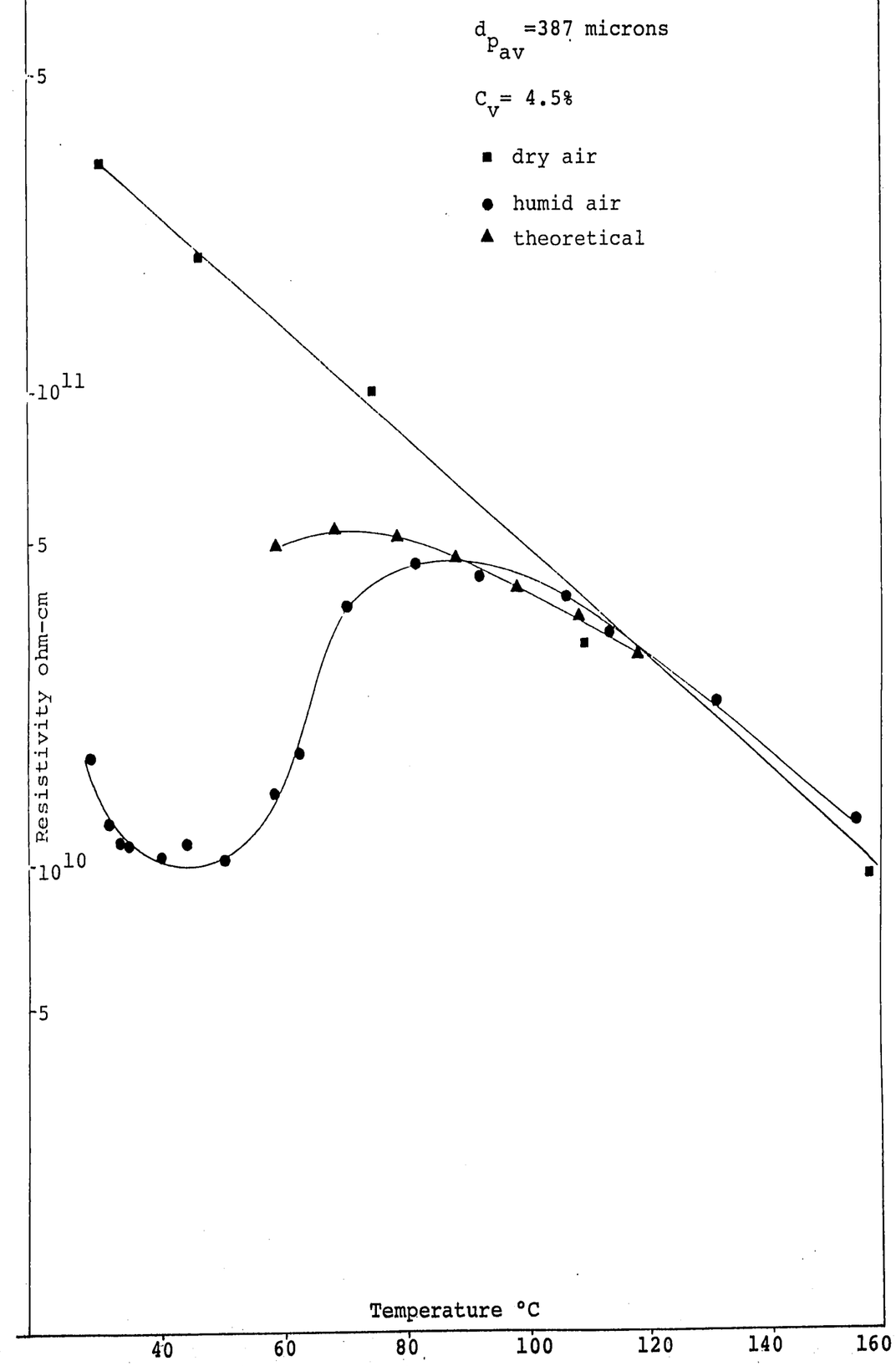
$d_{p_{av}}$ =387 microns
C_v= 4.5%
dry air
humid air
theoretical
5
10^{11}
5
10^{10}
5
Resistivity ohm-cm
Temperature °C
40
60
80
100
120
140
160

Figure 31

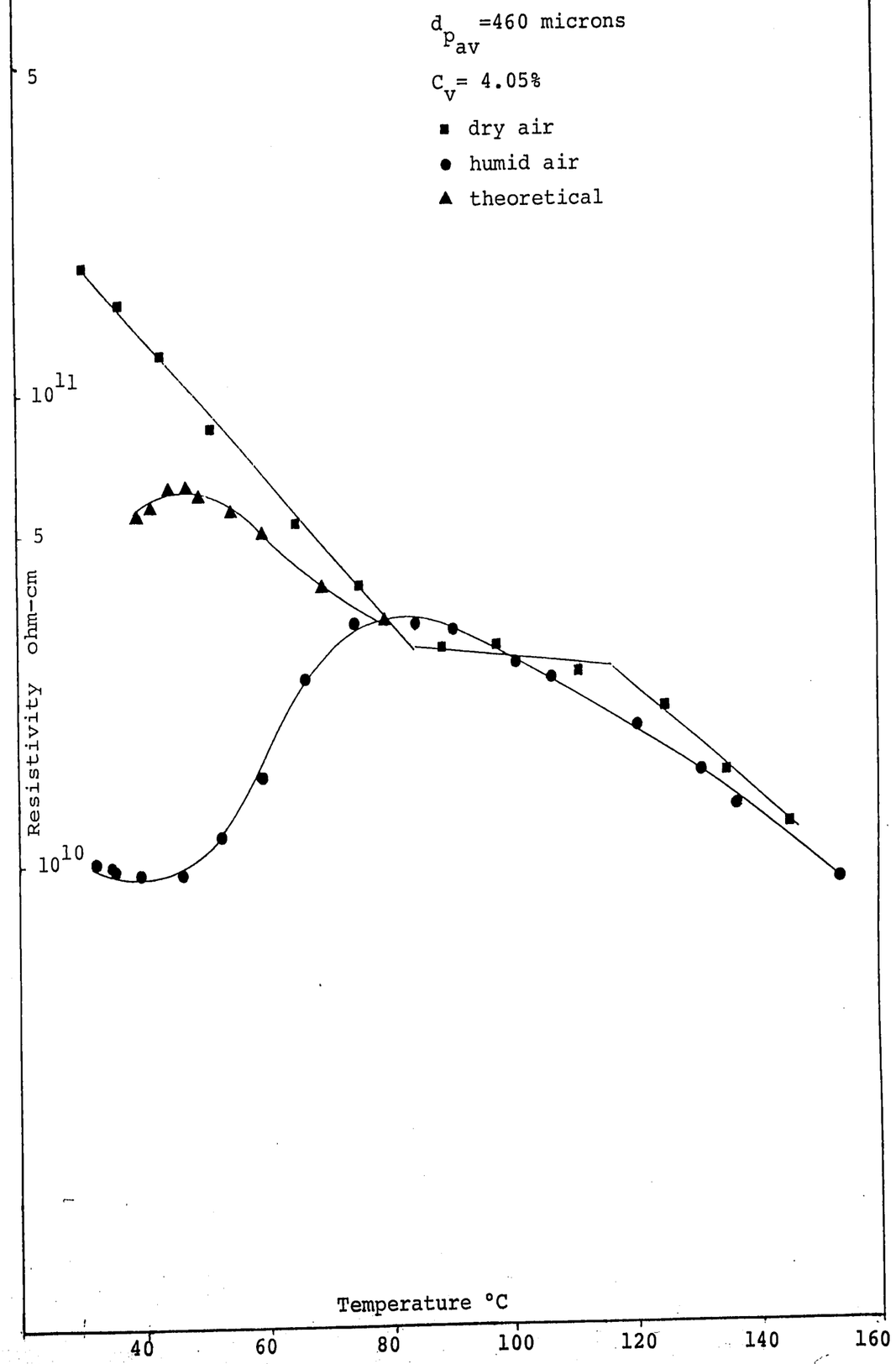
$d_{p_{av}}$ =460 microns
C_v= 4.05%
dry air
humid air
theoretical
5
10^{11}
5
10^{10}
Resistivity ohm-cm
Temperature °C
40
60
80
100
120
140
160

Figure 32

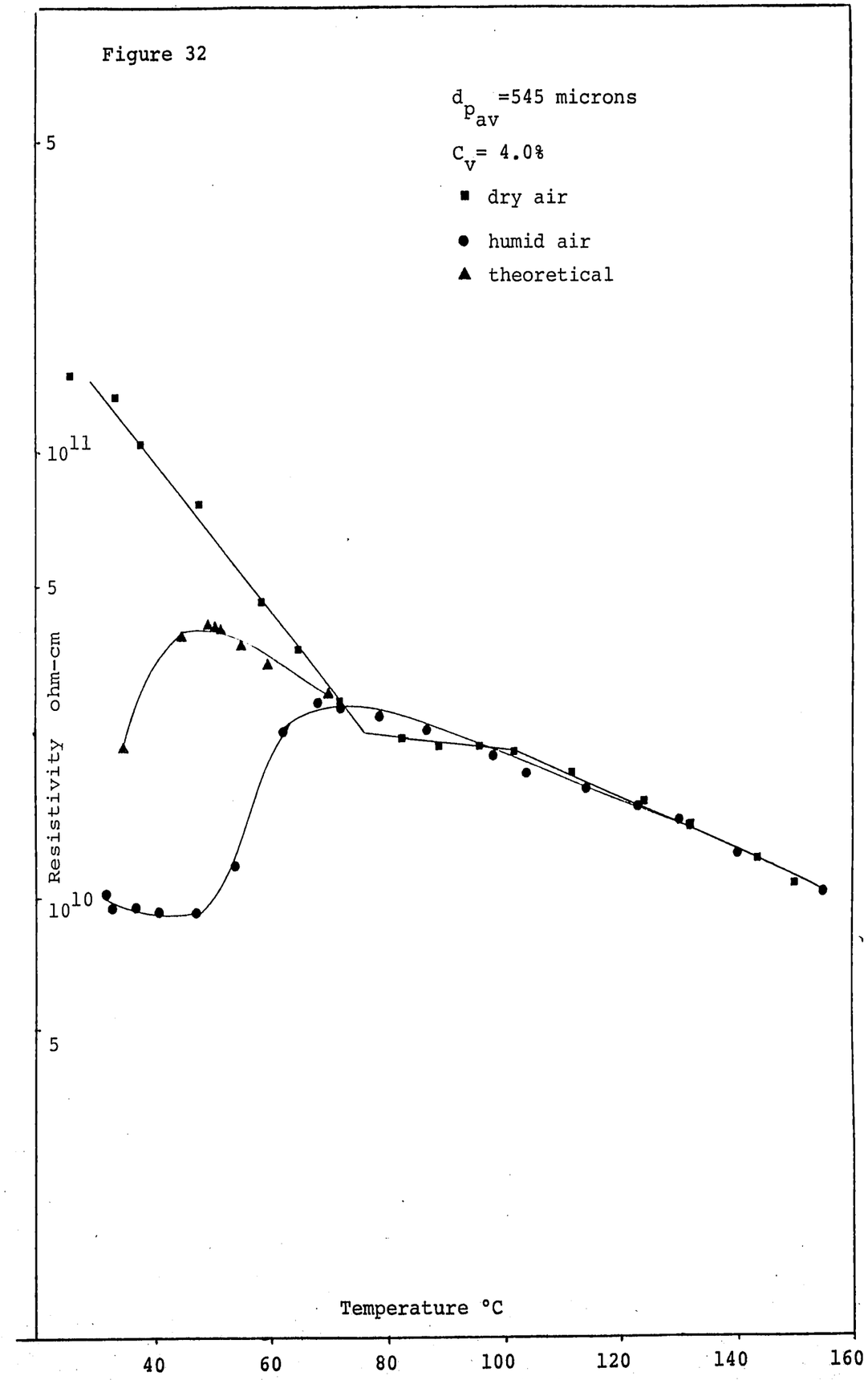
$d_{p_{av}}$ =545 microns
C_v= 4.0%
dry air
humid air
theoretical
5
10^{11}
5
10^{10}
5
Resistivity ohm-cm
Temperature °C
40
60
80
100
120
140
160

Figure 33

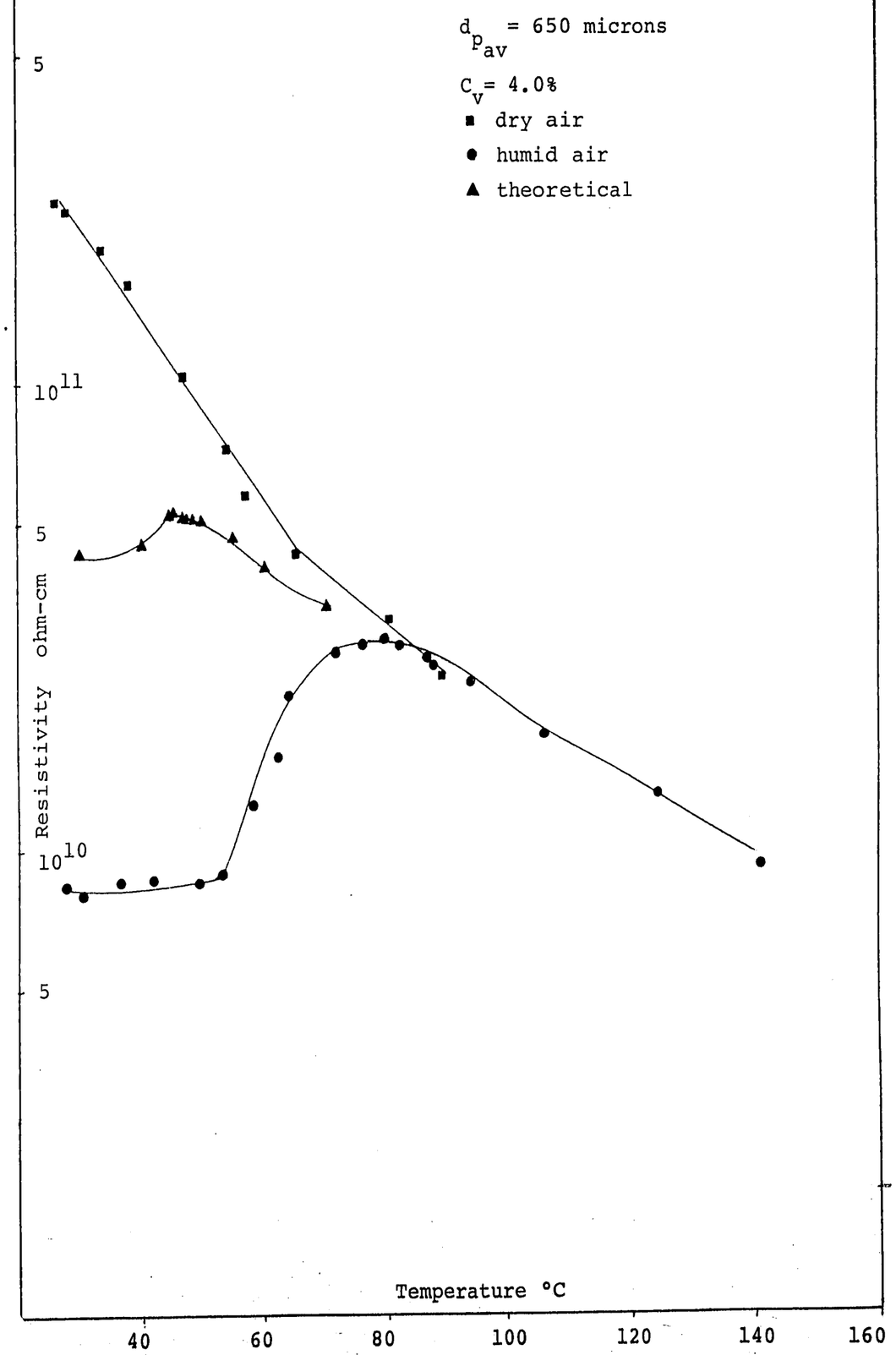
$d_{p_{av}}$ = 650 microns
C_v = 4.0%
dry air
humid air
theoretical
5
10^{11}
5
10^{10}
5
Resistivity ohm-cm
Temperature °C
40
60
80
100
120
140
160

Figure 33

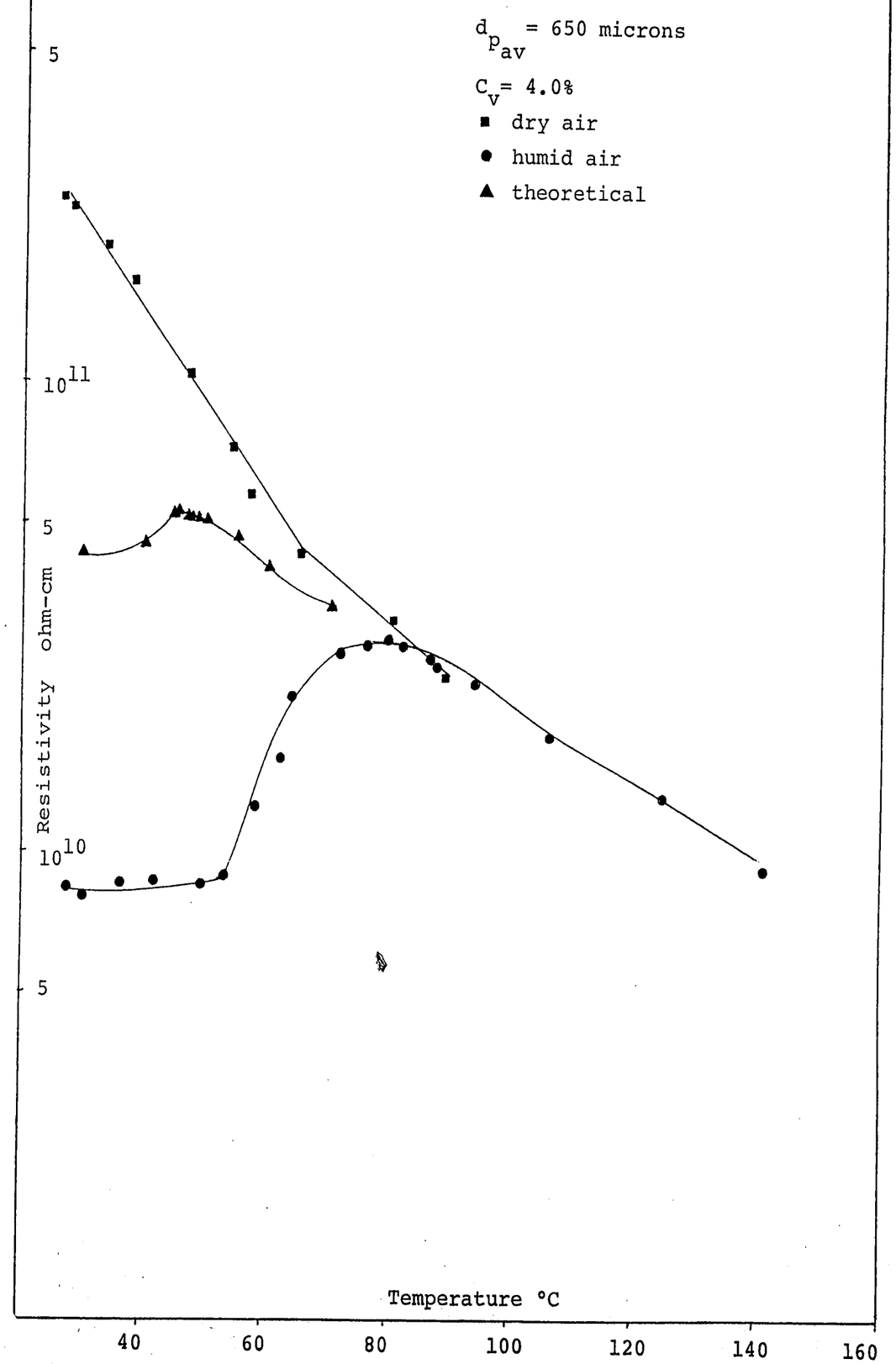
$d_{p_{av}}$ = 650 microns
C_v = 4.0%
dry air
humid air
theoretical
5
10^{11}
5
10^{10}
5
Resistivity ohm-cm
Temperature °C
40
60
80
100
120
140
160

Figure 34

$d_{p_{av}}$=387 microns $\quad$ p_k=.655 psi (T_{H_2O}=31.2°C)

From the experimental data find:

Maximum in humid curve, T=90°C
Intersection point of dry and humid curves, t=123°C

Evaluate p_0:

At T=90°C $\quad$ p_0=10.168 psi
At T=123°C $\quad$ p_0=32.760 psi

Evaluate $\emptyset$:

$$\emptyset=\ln\left(\frac{\ln(p/p_o)min}{\ln(p_k/p_o)}\right)=\ln\left(\frac{\ln(.655/32.760)}{\ln(.655/10.168)}\right)= 1.427$$

Evaluate K_s from $K=K_v+K_s\cdot\emptyset$:

$$K_s=\frac{K-K_v}{\emptyset} = \frac{\frac{1}{4.6x10^{10}}-\frac{1}{7.0x10^{10}}}{1.427} = 5.22x10^{-12}$$

For each T find p_o and calculate $\emptyset$ by:

$$\emptyset=\ln\left(\frac{-3.912}{\ln(.655/p_o)}\right)$$

Calculate $K_s\cdot\emptyset$:

$$K_s\cdot\emptyset= \emptyset\cdot 5.22x10^{-12}$$

Find value of K_v from graph:

Evaluate K:

$$K=K_v+K_s\cdot\emptyset$$

Take reciprocal of K:

$$=1/K$$

Figure 35

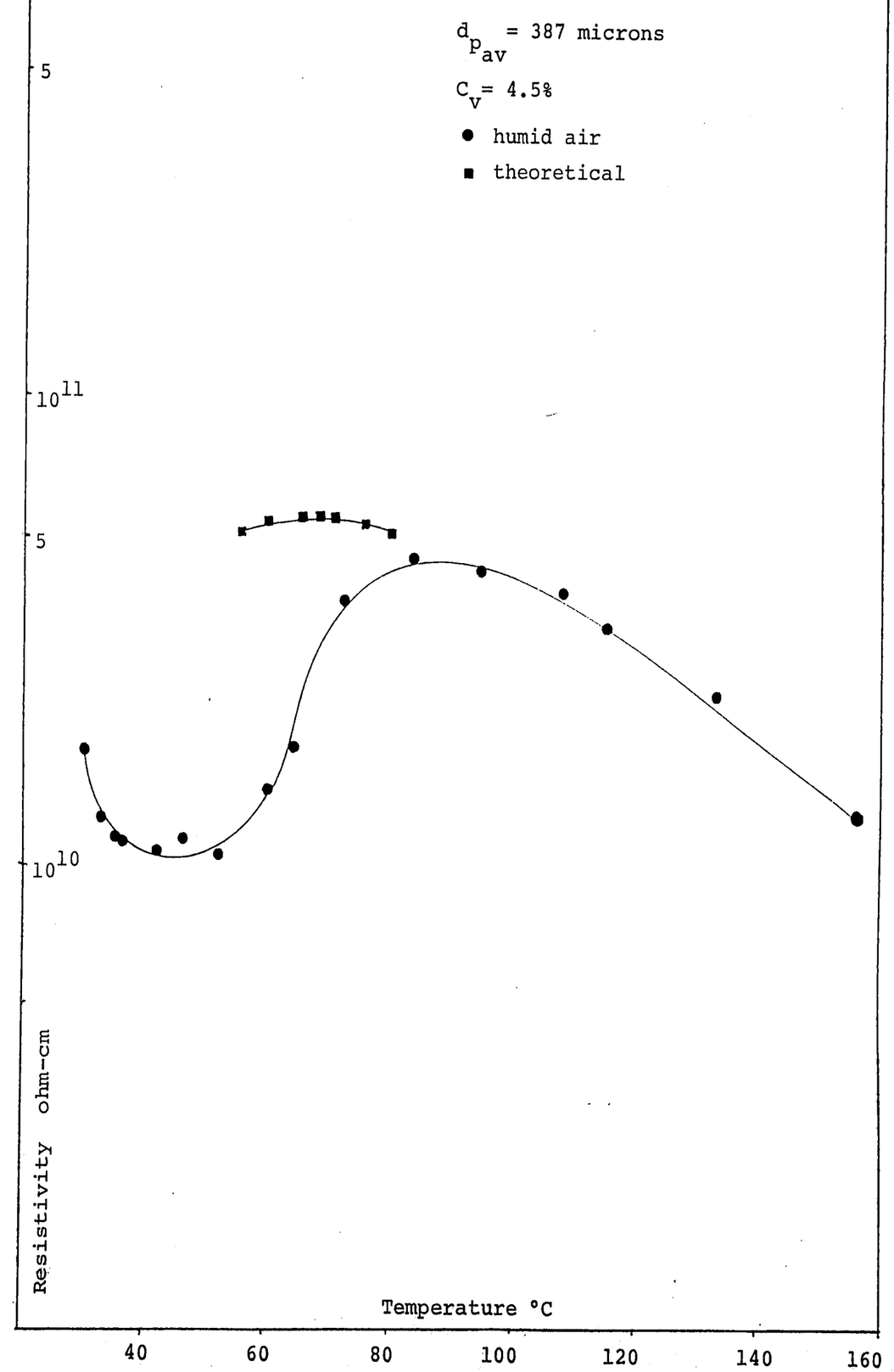
$d_{p_{av}}$ = 387 microns
C_v = 4.5%
● humid air
■ theoretical
5
10^{11}
5
10^{10}
Resistivity ohm-cm
Temperature °C
40
60
80
100
120
140
160

Figure 36

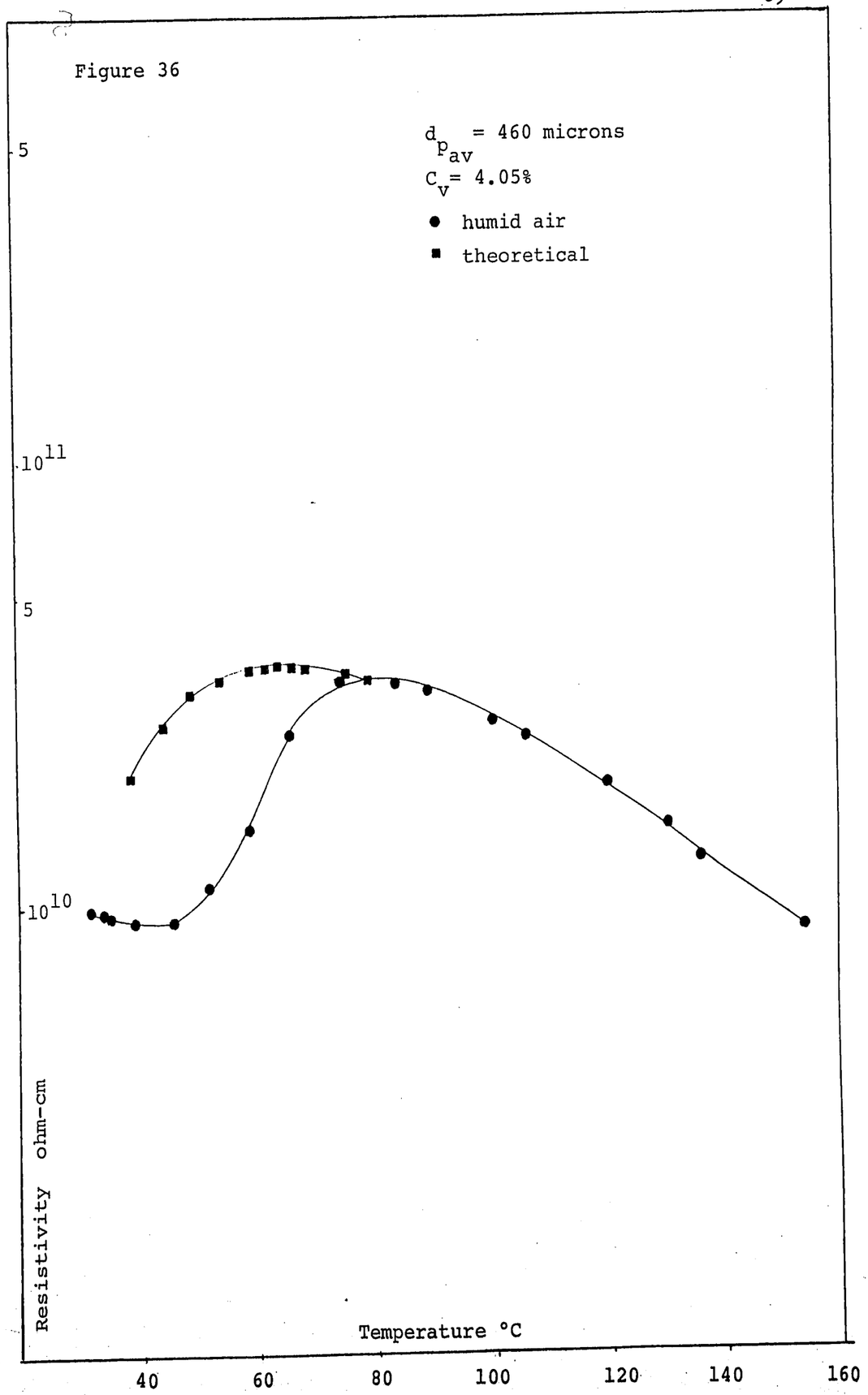
$d_{p_{av}}$ = 460 microns
C_v = 4.05%
humid air
theoretical
5
10^{11}
5
10^{10}
Resistivity ohm-cm
Temperature °C
40
60
80
100
120
140
160

Figure 37

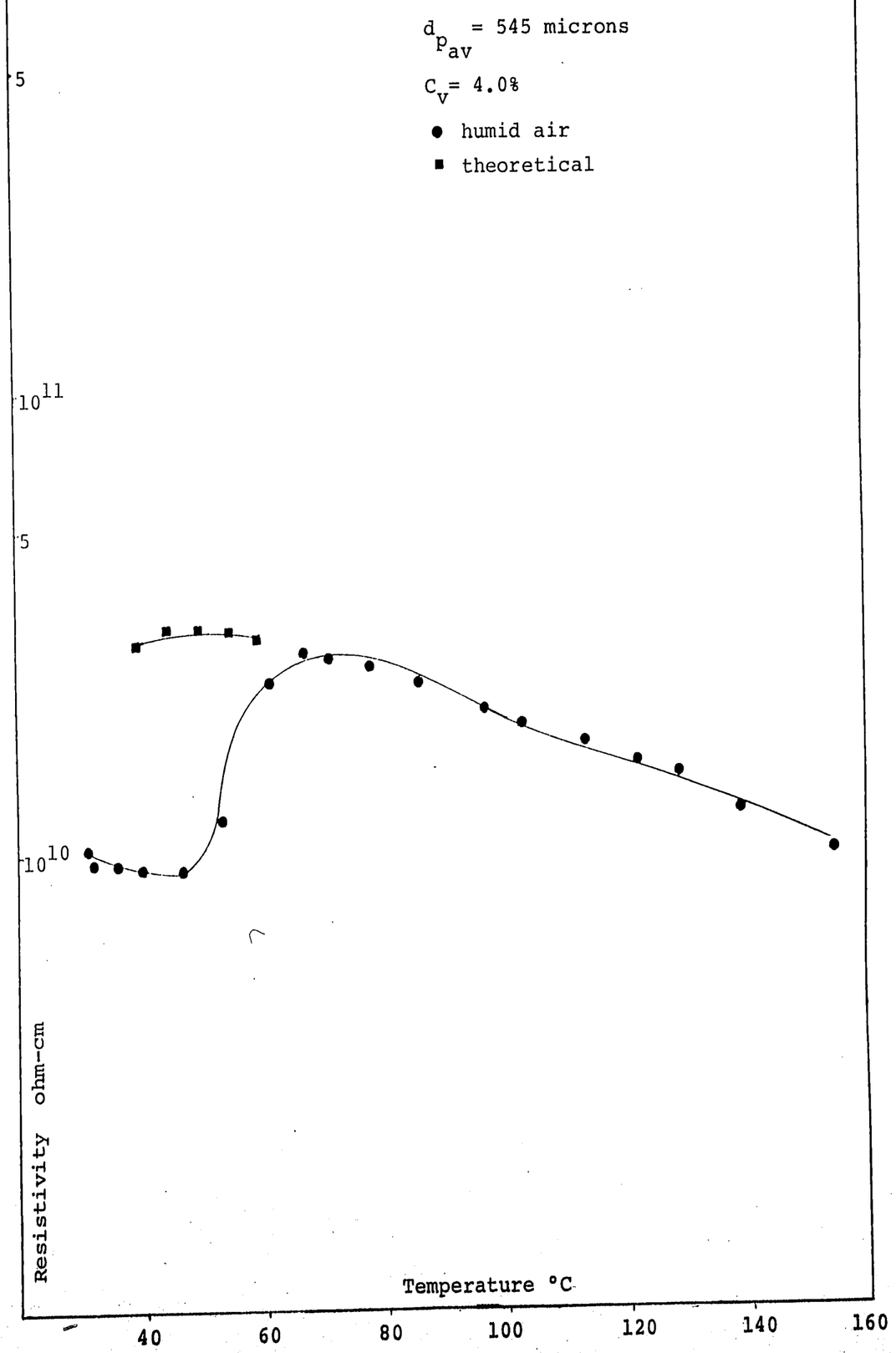
$d_{p_{av}}$ = 545 microns
C_v = 4.0%
● humid air
■ theoretical
5
10^{11}
5
10^{10}
Resistivity ohm-cm
Temperature °C
40
60
80
100
120
140
160

Figure 38

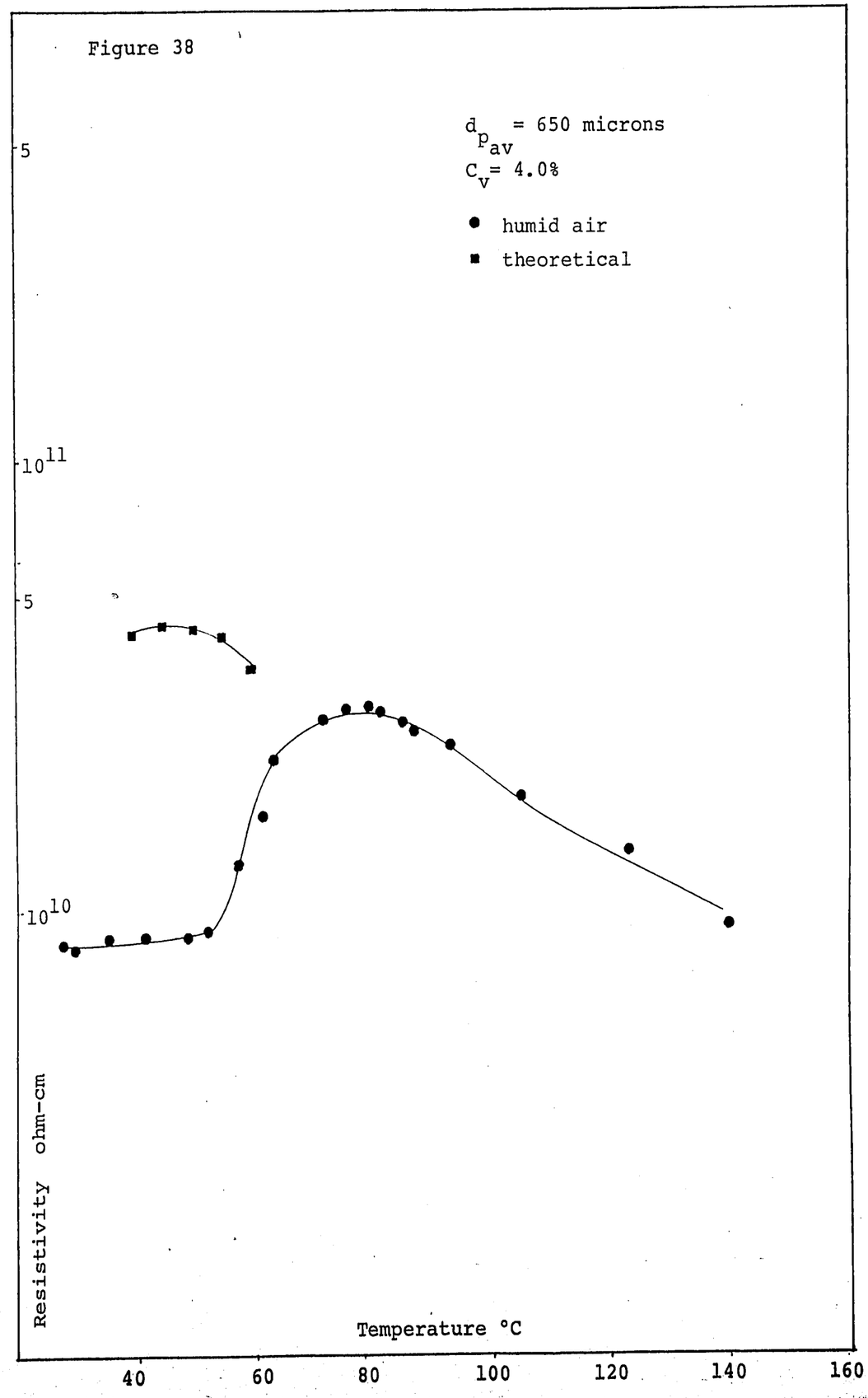
$d_{p_{av}}$ = 650 microns
C_v = 4.0%
humid air
theoretical
5
10^{11}
5
10^{10}
Resistivity ohm-cm
Temperature °C
40
60
80
100
120
140
160

Appendix C

Literature Cited

1. Minnick, L.J., Proc. Amer. Test. Mater. 1954, 54, 1129.

2. Watt, J.D. and Thorne, D.J., J. Applied Chemistry, 15(12), 585-594, (1965).

3. Goldstein, J.I., et. al., "Practical Scanning Electron Microscopy and Electron and Ion Microprobe Analysis." Chapter 11, Plenum Press, New York (1975).

4. Peters, D.G., et. al., "Chemical Separations and Measurements." Chapter 20, W. B. Saunders Co, Philadelphia (1974).

5. Private communication with Dr. B. Meyer, University of Washington.

6. Ditl, P. and Coughlin, R.W., "Improving Efficiency of Electrostatic Precipitation by Physicochemical Modification of the Electrical Resistivity of Flyash". To be published in the AIChE Journal. In press.